A new stabilized linear finite element method for solving reaction-convection-diffusion equations

Po-Wen Hsieh[a], Suh-Yuh Yang[b,*]

[a]*Department of Applied Mathematics, Chung Yuan Christian University, Jhongli District, Taoyuan City 32023, Taiwan*
[b]*Department of Mathematics, National Central University, Jhongli District, Taoyuan City 32001, Taiwan*

Abstract

In this paper, we propose a new stabilized linear finite element method for solving reaction-convection-diffusion equations with arbitrary magnitudes of reaction and diffusion. The key feature of the new method is that the test function in the stabilization term is taken in the adjoint-operator-like form $-\varepsilon\Delta v - (\boldsymbol{a}\cdot\nabla v)/\gamma + \sigma v$, where the parameter γ is appropriately designed to adjust the convection strength to achieve high accuracy and stability. We derive the stability estimates for the finite element solutions and establish the explicit dependence of L^2 and H^1 error bounds on the diffusivity, modulus of the convection field, reaction coefficient and the mesh size. The analysis shows that the proposed method is suitable for a wide range of mesh Péclet numbers and mesh Damköhler numbers. More specifically, if the diffusivity ε is sufficiently small with $\varepsilon < \|\boldsymbol{a}\|h$ and the reaction coefficient σ is large enough such that $\|\boldsymbol{a}\| < \sigma h$, then the method exhibits optimal convergence rates in both L^2 and H^1 norms. However, for a small reaction coefficient satisfying $\|\boldsymbol{a}\| \geq \sigma h$, the method behaves like the well-known streamline upwind/Petrov-Galerkin formulation of Brooks and Hughes. Several numerical examples exhibiting boundary or interior layers are given to demonstrate the high performance of the proposed method. Moreover, we apply the developed method to time-dependent reaction-convection-diffusion problems and simulation results show the efficiency of the approach.

Keywords: reaction-convection-diffusion equation; boundary layer; interior layer; stabilized finite element method; stabilization parameter.

2000 MSC: 65N12, 65N15, 65N30

1. Introduction

In this paper, we are interested in the stabilized linear finite element approximations to the following Dirichlet boundary value problem for the reaction-convection-diffusion equation:

$$\begin{cases} -\varepsilon\Delta u + \boldsymbol{a}\cdot\nabla u + \sigma u &=& f & \text{in } \Omega, \\ u &=& 0 & \text{on } \partial\Omega, \end{cases} \tag{1}$$

where $\Omega \subset \mathbb{R}^2$ is an open bounded convex polygonal domain with boundary $\partial\Omega$, u is the physical quantity of interest (e.g., temperature in heat conduction or concentration of some chemical substance), $0 < \varepsilon \leq 1$ is the constant diffusivity, $\boldsymbol{a} \in (H^1(\Omega) \cap L^\infty(\Omega))^2$ is the given convection (velocity) field satisfying $\nabla \cdot \boldsymbol{a} = 0$ in Ω, $\sigma \geq 0$ is the constant reaction coefficient, and $f \in L^2(\Omega)$ is the given source function. It is well known that when the diffusivity ε is relatively small compared with the modulus of the convection field $\boldsymbol{a}$ or the reaction coefficient σ, the solution u of problem (1) may exhibit localized phenomena such as boundary and interior layers [1, 2, 3, 4, 5]. Boundary and

interior layers are some narrow regions in the immediate vicinity of the domain boundary $\partial\Omega$ or in the interior of the domain Ω where the solution has large gradients. It is often difficult to numerically resolve the solution within the neighborhood of the layer regions, and the conventional numerical methods usually produce low accuracy or suffer from instability [1, 2, 3, 4, 5]. For instance, the standard Galerkin method using continuous piecewise linear (P_1) or bilinear (Q_1) elements performs very poorly since large spurious oscillations exhibit not only in the layer regions but also in other regions. Therefore, in the past three decades, a large class of the so-called stabilized finite element methods (FEMs) has been intensively developed to overcome this difficulty, see, e.g., [6, 7, 8, 9, 10, 11, 12, 13]. The stabilized FEMs are formed by adding to the standard Galerkin method some consistent variational terms, relating to the residuals of the partial differential equations, which involve some mesh-dependent stabilization parameters. A robust approach for the derivation of such a stabilized FEM is motivated by the bubble-enriched method [14, 15, 16, 17] combined with the procedure of static condensation [18]. It is now clear that the stabilization parameters play the key roles in the stabilization method. To a great degree, they account for why those additional stabilization terms not only can enhance the numerical stability but also can improve the accuracy in the finite element solutions.

In this paper, we will focus on developing efficient stabilized FEMs for solving the reaction-convection-diffusion problem (1). First, let us give a brief review of some previous works, which are closely related with the new method that we will introduce in this paper. In [18], Franca and Farhat proposed a so-called unusual stabilized linear FEM for problem (1) with vanishing convection field $\boldsymbol{a}$. They proved that the error estimate is optimal in H^1-seminorm independent of the values of ε and σ. In addition, for $\varepsilon \leq \sigma h_T^2$ for all elements, optimal order in L^2 norm can also be obtained without using the duality argument. They also considered the problem (1) including the convection term $\boldsymbol{a} \cdot \nabla u$ and suggested a stabilization parameter to deal with all the three effects from reaction, convection and diffusion simultaneously, but no analysis is given therein. In [19], Franca and Valentin constructed a new stabilization parameter for the presence of the convection term to improve the accuracy. The improvement is also justified therein from an error analysis. Some further results have also been achieved by Duan [20]. In [21], Hauke, Sangalli and Doweidar proposed an efficient stabilized FEM for solving the reaction-convection-diffusion problems. Their method combines two types of stabilization integrals, namely an adjoint stabilization and a gradient adjoint stabilization, and two stabilization parameters are involved therein. These two parameters are chosen based on imposing one-dimensional nodal exactness. More recently, we devised a new stabilized FEM for problem (1) in [22], with emphasis on the case of small diffusivity ε and large reaction coefficient σ. As usual, we employed the continuous piecewise P_1 (or Q_1) elements and used the residual of the differential equation in problem (1) to define the stabilization term, but in which a novel stabilization parameter is carefully designed. The main differences from the stabilization methods proposed in [18] and [19] are that the stabilization parameter is deterministic and explicit, without the comparisons among the three effect-terms: reaction, convection and diffusion; the stabilization parameter is always the same no matter if the convection $\boldsymbol{a}$ is present or not in problem (1); and the test function involved in the stabilization term is taken in the form $-\varepsilon\Delta v + \sigma v$, instead of the adjoint-operator form $-\varepsilon\Delta v - \boldsymbol{a} \cdot \nabla v + \sigma v$ in [18] and [19]. The stabilized linear FEM proposed in [22] has been proved to be very effective for problem (1) with a small diffusivity ε and a large reaction coefficient σ.

In this paper, we will propose a new stabilized linear FEM for solving reaction-convection-diffusion equations with arbitrary magnitudes of reaction and diffusion. The key feature of the new method is that the test function in

the stabilization term is taken in the adjoint-operator-like form $-\varepsilon \Delta v - (\boldsymbol{a} \cdot \nabla v)/\gamma + \sigma v$, where the stabilization parameter γ will be appropriately designed to adjust the convection strength to achieve high accuracy and stability. We will explicitly establish the dependence of L^2 and H^1 error bounds on the diffusivity ε, modulus of the convection field, given as $\|\boldsymbol{a}\| := \mathrm{ess\,sup}_{(x,y)\in\Omega}(a_1^2(x,y) + a_2^2(x,y))^{1/2}$, reaction coefficient σ and the mesh size h. Our analysis shows that the proposed method is suitable for a wide range of mesh Péclet numbers, defined as $Pe_h := \|\boldsymbol{a}\|h/(2\varepsilon)$, and mesh Damköhler numbers, given by $Da_h := \sigma h/\|\boldsymbol{a}\|$. More specifically, if the diffusivity ε is sufficiently small with $\varepsilon < \|\boldsymbol{a}\|h$ (i.e., $Pe_h > 1/2$) and the reaction coefficient σ is large enough such that $\|\boldsymbol{a}\| < \sigma h$ (i.e., $Da_h > 1$), then the proposed method exhibits optimal convergence rates in both L^2 and H^1 norms, with respect to the mesh size as well as the regularity of the exact solution; see Remark 3 in Section 3 below. On the other hand, for a small reaction coefficient satisfying $\|\boldsymbol{a}\| \geq \sigma h$ (i.e., $Da_h \leq 1$), the proposed method behaves like the well-known streamline upwind/Petrov-Galerkin (SUPG) formulation of Brooks and Hughes [6]. We will present several numerical examples involving boundary or interior layers to demonstrate the high performance of the proposed stabilized linear FEM. The numerical results obtained are also compared with those of our previous stabilized FEM [22]. Strong numerical evidences indicate that the proposed stabilization method is more stable than that of [22]. Moreover, we will apply the developed method to the time-dependent reaction-convection-diffusion problems and numerical results will be reported to illustrate the effectiveness of the proposed approach. Finally, we remark that the present new method can work well on unstructured adaptive meshes, provided the stabilization parameters are directly redefined element-by-element (cf. Remark 1 in Section 2). This expectation will be confirmed by numerical experiments.

The remainder of this paper is organized as follows. In Section 2, we introduce the new stabilized linear FEM and establish the stability estimates for the finite element solutions. In Section 3, error estimates in L^2 and H^1 norms are derived, where the dependence of error bounds on the diffusivity, modulus of the convection field, reaction coefficient and the mesh size are given. In Section 4, several numerical examples are presented to illustrate the effectiveness of the proposed method. In Section 5, we apply the developed method to time-dependent reaction-convection-diffusion problems. Finally, a summary and conclusions are drawn in Section 6.

2. The stabilized linear finite element method and its stability estimates

Throughout this paper, we will use the standard notation and definitions for the Sobolev spaces $H^m(\Omega)$ for nonnegative integers m (cf. [1, 23, 24, 25]). The associated inner product and norm are denoted by $(\cdot,\cdot)_m$ and $\|\cdot\|_m$, respectively. As usual, $L^2(\Omega) = H^0(\Omega)$ and

$$H_0^1(\Omega) = \{v \in H^1(\Omega) : v = 0 \text{ on } \partial\Omega\}.$$

Let $\{\mathcal{T}_h\}_{0<h\leq 1}$ be a family of triangulations of Ω. A triangulation $\mathcal{T}_h$ of Ω into elements T consisting of triangles or quadrilaterals is performed in the usual way; the intersection of any two elements is a vertex, or an edge or empty, and $\overline{\Omega} = \cup_{T\in\mathcal{T}_h}T$. For each triangulation the subscript $h \in (0,1]$ refers to the level of refinement of the triangulation. In particular, the mesh size h is defined as $h = \max\{h_T : T \in \mathcal{T}_h\}$, where h_T denotes the diameter of element T. We always assume that the family $\{\mathcal{T}_h\}_{0<h\leq 1}$ of triangulations is shape regular [1, 23, 24]. Moreover, let $(\cdot,\cdot)_{m,T}$ and $\|\cdot\|_{m,T}$ denote the associated inner product and norm in $H^m(T)$, respectively, where T is a given element in $\mathcal{T}_h$.

Let $\mathcal{V}_1 \subseteq H_0^1(\Omega)$ be the continuous piecewise linear (P_1) or bilinear (Q_1) finite element space over the triangulation $\mathcal{T}_h$. The standard interpolation theory [23, 24] ensures that if $u \in H^2(\Omega) \cap H_0^1(\Omega)$ then there exists an interpolation $\mathcal{I}_h u \in \mathcal{V}_1$ such that

$$\|u - \mathcal{I}_h u\|_0 + h\|u - \mathcal{I}_h u\|_1 + h^2\|u - \mathcal{I}_h u\|_2 \leq Ch^2\|u\|_2, \tag{2}$$

where C is a positive constant independent of h. In this paper, we use C to denote a generic positive constant, possibly different at different occurrences, which is always independent of h and other parameters introduced.

We now propose the following new stabilized linear FEM for approximating problem (1):

$$\text{Find } u_h \in \mathcal{V}_1 \text{ such that } B(u_h, v_h) = L(v_h) \quad \forall \, v_h \in \mathcal{V}_1, \tag{3}$$

where the bilinear form $B(\cdot, \cdot)$ and the linear form $L(\cdot)$ are respectively defined as

$$B(u, v) \quad := \quad \varepsilon(\nabla u, \nabla v)_0 + (\boldsymbol{a} \cdot \nabla u, v)_0 + \sigma(u, v)_0 - \sum_{T \in \mathcal{T}_h} \tau\left(-\varepsilon\Delta u + \boldsymbol{a} \cdot \nabla u + \sigma u, -\varepsilon\Delta v - \frac{\boldsymbol{a} \cdot \nabla v}{\gamma} + \sigma v\right)_{0,T}, \tag{4}$$

$$L(v) \quad := \quad (f, v)_0 - \sum_{T \in \mathcal{T}_h} \tau\left(f, -\varepsilon\Delta v - \frac{\boldsymbol{a} \cdot \nabla v}{\gamma} + \sigma v\right)_{0,T}, \tag{5}$$

and the stabilization parameters τ and γ are given by

$$\tau \quad = \quad \frac{h^2 \xi_2}{\sigma h^2 \xi_1 + 8\varepsilon + 2\|\boldsymbol{a}\|h}, \tag{6}$$

$$\gamma \quad = \quad \begin{cases} 1 & \text{if } \|\boldsymbol{a}\| \geq \sigma h, \\ \max\left\{\dfrac{h^2 + 2\|\boldsymbol{a}\|h/\sigma}{h^2(\xi_1 - 1) + 8\varepsilon/\sigma}, \dfrac{h^2(\xi_1 - 1) + 8\varepsilon/\sigma}{h^2 + 2\|\boldsymbol{a}\|h/\sigma}\right\} & \text{if } \|\boldsymbol{a}\| < \sigma h, \end{cases} \tag{7}$$

with $\|\boldsymbol{a}\| := \text{ess sup}_{(x,y) \in \Omega} \sqrt{a_1^2(x, y) + a_2^2(x, y)}$,

$$\xi_1 := \begin{cases} 1 & \text{if } \sigma = 0, \\ \max\left\{1, \dfrac{8\varepsilon}{\sigma h^2}\right\} & \text{if } \sigma \neq 0, \end{cases} \quad \text{and} \quad \xi_2 := \begin{cases} 1 & \text{if } \|\boldsymbol{a}\| \geq \sigma h, \\ 1 + \dfrac{2\|\boldsymbol{a}\|}{\sigma h} & \text{if } \|\boldsymbol{a}\| < \sigma h. \end{cases} \tag{8}$$

Notice that $\tau, \gamma > 0$ and $\xi_1, \xi_2 \geq 1$. Here, we emphasize that the test function in the stabilization term is taken in the adjoint-operator-like form "$-\varepsilon\Delta v - (\boldsymbol{a} \cdot \nabla v)/\gamma + \sigma v$", which makes us able to adjust the convection strength through the stabilization parameter γ to achieve high accuracy and stability of the method (3). This feature is the main difference from the previous stabilization methods studied in [18, 19, 20, 21, 22]. We also remark that in (4) and (5), we have $\Delta v_h|_T = 0$ for all $v_h \in \mathcal{V}_1$ and $T \in \mathcal{T}_h$, since each v_h is a piecewise linear (bilinear) function. However, we still retain the terms therein for the clarity of presentation.

We have the following stability estimate of the stabilized linear FEM (3):

Lemma 1. *The stability estimate holds: for all $v_h \in \mathcal{V}_1$, we have*

$$B(v_h, v_h) = \begin{cases} \varepsilon\|\nabla v_h\|_0^2 + \dfrac{\sigma^2 h^2(\xi_1 - 1) + 8\sigma\varepsilon + 2\sigma\|\boldsymbol{a}\|h}{\sigma h^2 \xi_1 + 8\varepsilon + 2\|\boldsymbol{a}\|h}\|v_h\|_0^2 + \dfrac{h^2}{\sigma h^2 \xi_1 + 8\varepsilon + 2\|\boldsymbol{a}\|h}\|\boldsymbol{a} \cdot \nabla v_h\|_0^2 & \text{if } \|\boldsymbol{a}\| \geq \sigma h, \\[4mm] \varepsilon\|\nabla v_h\|_0^2 + \dfrac{\sigma^2 h^2(\xi_1 - 1) + 8\sigma\varepsilon}{\sigma h^2 \xi_1 + 8\varepsilon + 2\|\boldsymbol{a}\|h}\|v_h\|_0^2 + \dfrac{h^2 + 2\|\boldsymbol{a}\|h/\sigma}{(\sigma h^2 \xi_1 + 8\varepsilon + 2\|\boldsymbol{a}\|h)\gamma}\|\boldsymbol{a} \cdot \nabla v_h\|_0^2 & \text{if } \|\boldsymbol{a}\| < \sigma h. \end{cases} \tag{9}$$

4

Proof. First, we note that from Green's formula [25] with the fact that $\nabla \cdot \boldsymbol{a} = 0$ in Ω, we have $(\boldsymbol{a} \cdot \nabla v_h, v_h)_0 = 0$ for all $v_h \in \mathcal{V}_1$. If $\sigma = 0$, then $\xi_1 = 1$, $\xi_2 = 1$ and $\gamma = 1$ and the first part in (9) can be immediately obtained. We consider the case of $\sigma > 0$. From (4) and (6), we have

$$
\begin{aligned}
B(v_h, v_h) &= \varepsilon \|\nabla v_h\|_0^2 + (\boldsymbol{a} \cdot \nabla v_h, v_h)_0 + \sigma \|v_h\|_0^2 - \sum_{T \in \mathcal{T}_h} \tau \Big(\boldsymbol{a} \cdot \nabla v_h + \sigma v_h, -\frac{\boldsymbol{a} \cdot \nabla v_h}{\gamma} + \sigma v_h \Big)_{0,T} \\
&= \varepsilon \|\nabla v_h\|_0^2 + \frac{\sigma^2 h^2(\xi_1 - \xi_2) + 8\sigma\varepsilon + 2\sigma\|\boldsymbol{a}\|h}{\sigma h^2 \xi_1 + 8\varepsilon + 2\|\boldsymbol{a}\|h} \sum_{T \in \mathcal{T}_h} \|v_h\|_{0,T}^2 + \frac{h^2 \xi_2}{(\sigma h^2 \xi_1 + 8\varepsilon + 2\|\boldsymbol{a}\|h)\gamma} \sum_{T \in \mathcal{T}_h} \|\boldsymbol{a} \cdot \nabla v_h\|_{0,T}^2 \\
&\quad - \frac{\sigma h^2 \xi_2}{\sigma h^2 \xi_1 + 8\varepsilon + 2\|\boldsymbol{a}\|h} \sum_{T \in \mathcal{T}_h} (\boldsymbol{a} \cdot \nabla v_h, v_h)_{0,T} + \frac{\sigma h^2 \xi_2}{(\sigma h^2 \xi_1 + 8\varepsilon + 2\|\boldsymbol{a}\|h)\gamma} \sum_{T \in \mathcal{T}_h} (v_h, \boldsymbol{a} \cdot \nabla v_h)_{0,T},
\end{aligned}
$$

which, combining with

$$
\sum_{T \in \mathcal{T}_h} (\boldsymbol{a} \cdot \nabla v_h, v_h)_{0,T} = \sum_{T \in \mathcal{T}_h} (v_h, \boldsymbol{a} \cdot \nabla v_h)_{0,T} = (\boldsymbol{a} \cdot \nabla v_h, v_h)_0 = 0
$$

and (7), (8), easily implies (9). This completes the proof. $\square$

The stability estimate (9) ensures the unique solvability of the stabilized linear FEM (3). We note that the stabilization parameters τ and γ given in (6) and (7) are defined globally, which may be not suitable for unstructured and adaptive meshes. However, if the stabilization parameters are directly redefined element-by-element, as we will see in Remark 1 below, the resulting stabilized linear FEM can work very well for adaptive computations; see numerical results reported in Section 4 and Section 5. This advantage makes the newly proposed method different from that of our previous method [22]. We also remark that the stabilized linear FEM (3) is a consistent formulation, since the equation in (3) is satisfied when the finite element solution u_h is replaced by the exact solution u of problem (1). As a result, we have the following orthogonality property:

$$
B(u - u_h, v_h) = 0 \quad \forall\, v_h \in \mathcal{V}_1, \tag{10}
$$

which plays an important role in the error estimates of the stabilized linear FEM (3) given in Section 3.

Remark 1. For applying the stabilized linear FEM (3) to the computations on unstructured and adaptive meshes, we therefore define the following elementwise stabilization parameters:

$$
\tau_T = \frac{h_T^2 \xi_{2T}}{\sigma h_T^2 \xi_{1T} + 8\varepsilon + 2\|\boldsymbol{a}\|_T h_T}, \quad \forall\, T \in \mathcal{T}_h, \tag{11}
$$

$$
\gamma_T = \begin{cases} 1 & \text{if } \|\boldsymbol{a}\|_T \geq \sigma h_T, \\ \max\Big\{ \dfrac{h_T^2 + 2\|\boldsymbol{a}\|_T h_T/\sigma}{h_T^2(\xi_{1T} - 1) + 8\varepsilon/\sigma}, \dfrac{h_T^2(\xi_{1T} - 1) + 8\varepsilon/\sigma}{h_T^2 + 2\|\boldsymbol{a}\|_T h_T/\sigma} \Big\} & \text{if } \|\boldsymbol{a}\|_T < \sigma h_T, \end{cases} \quad \forall\, T \in \mathcal{T}_h, \tag{12}
$$

where $\|\boldsymbol{a}\|_T := \operatorname{ess\,sup}_{(x,y) \in T} \sqrt{a_1^2(x,y) + a_2^2(x,y)}$,

$$
\xi_{1T} := \begin{cases} 1 & \text{if } \sigma = 0, \\ \max\Big\{ 1, \dfrac{8\varepsilon}{\sigma h_T^2} \Big\} & \text{if } \sigma \neq 0, \end{cases} \quad \text{and} \quad \xi_{2T} := \begin{cases} 1 & \text{if } \|\boldsymbol{a}\|_T \geq \sigma h_T, \\ 1 + \dfrac{2\|\boldsymbol{a}\|_T}{\sigma h_T} & \text{if } \|\boldsymbol{a}\|_T < \sigma h_T, \end{cases} \quad \forall\, T \in \mathcal{T}_h.
$$

Now, if the global parameters τ and γ in (4) and (5) are replaced by the elementwise defined stabilization parameters τ_T and γ_T for all $T \in \mathcal{T}_h$, then we can prove the following stability estimate: *Assume that $\sigma = 0$ or the diffusivity ε is*

sufficiently small such that $\varepsilon < |\boldsymbol{a}\|_T h_T$ and the reaction coefficient σ is large enough with $\|\boldsymbol{a}\|_T < \sigma h_T$ for all $T \in \mathcal{T}_h$. Then we have

$$B(v_h, v_h) \geq \varepsilon \|\nabla v_h\|_0^2 \quad \forall v_h \in \mathcal{V}_1. \tag{13}$$

The stability estimate (13) is somewhat weaker than that in Lemma 1. Its proof is based on Hölder's inequality and Young's inequality with direct computations. We omit the details here.

Remark 2 (Duan-Hsieh-Tan-Yang stabilized linear FEM). In our previous work [22], we have proposed the following stabilization method using continuous piecewise P_1 (or Q_1) elements:

$$Find \ u_h \in \mathcal{V}_1 \ such \ that \ B_{DHTY}(u_h, v_h) = L_{DHTY}(v_h) \quad \forall v_h \in \mathcal{V}_1, \tag{14}$$

where the bilinear form $B_{DHTY}(\cdot, \cdot)$ and the linear form $L_{DHTY}(\cdot)$ are, respectively, defined as follows:

$$B_{DHTY}(u, v) \quad := \quad \varepsilon(\nabla u, \nabla v)_0 + (\boldsymbol{a} \cdot \nabla u, v)_0 + \sigma(u, v)_0 - \sum_{T \in \mathcal{T}_h} \tau \big(-\varepsilon \Delta u + \boldsymbol{a} \cdot \nabla u + \sigma u, -\varepsilon \Delta v + \sigma v\big)_{0,T},$$

$$L_{DHTY}(v) \quad := \quad (f, v)_0 - \sum_{T \in \mathcal{T}_h} \tau \big(f, -\varepsilon \Delta v + \sigma v\big)_{0,T},$$

and the single stabilization parameter τ is globally defined by

$$\tau = \frac{h^2}{\sigma h^2 + 6\varepsilon}.$$

The most important feature of the method is that the test function in the stabilization term is taken in the form $-\varepsilon \Delta v + \sigma v$, instead of the adjoint-operator form $-\varepsilon \Delta v - \boldsymbol{a} \cdot \nabla v + \sigma v$ in [18] and [19]. This stabilized linear FEM has been shown to be very effective for problems with a small diffusivity ε and a large reaction coefficient σ. In adaptive computations, the stabilization parameter τ in the method (14) should be directly replaced by its elementwise version,

$$\tau_T = \frac{h_T^2}{\sigma h_T^2 + 6\varepsilon} \quad \forall T \in \mathcal{T}_h. \tag{15}$$

However, with this elementwise defined stabilization parameter (15), it seems not easy to derive a stability estimate similar to (13). Notice that when the diffusivity $\varepsilon \to 0^+$ and the reaction coefficient $\sigma \to \infty$, we have $\gamma_T \to \infty$ for all $T \in \mathcal{T}_h$ and then methods (3) and (14) have the almost identical test functions in the stabilization terms, since $-\varepsilon \Delta v - (\boldsymbol{a} \cdot \nabla v)/\gamma_T + \sigma v \approx -\varepsilon \Delta v + \sigma v$ for all $v \in \mathcal{V}_1$. This gives us a clue why γ_T plays an important role in the newly proposed stabilized linear FEM for obtaining stability estimate (13) in adaptive computations.

3. Error estimates of the stabilized linear FEM

We now proceed to estimate the errors of the finite element solution u_h of the newly proposed stabilized linear FEM (3). We will explicitly establish the dependence of L^2 and H^1 error bounds on the diffusivity ε, modulus of the convection field $\|\boldsymbol{a}\|$, reaction coefficient σ and the mesh size h. The main results can be stated as follows:

Theorem 2. *Let $u \in H_0^1(\Omega) \cap H^2(\Omega)$ be the solution of problem (1) and $u_h \in \mathcal{V}_1 \subseteq H_0^1(\Omega)$ be the stabilized linear finite element solution defined by (3). Then there exists a constant $C > 0$ independent of ε, $\boldsymbol{a}$, σ and h such that*

$$
\|\nabla u - \nabla u_h\|_0 \leq
\begin{cases}
C\left(h + h^{3/2}\sqrt{\dfrac{\|\boldsymbol{a}\|}{\varepsilon}}\right)\|u\|_2 & \text{if } \|\boldsymbol{a}\| \geq \sigma h, \\[4mm]
Ch\,\|u\|_2 & \text{if } \|\boldsymbol{a}\| < \sigma h,
\end{cases}
\tag{16}
$$

$$
\|u - u_h\|_0 \leq C\left(h^2 + h\sqrt{\dfrac{\varepsilon}{\sigma}}\right)\|u\|_2 \qquad \text{if } \|\boldsymbol{a}\| < \sigma h.
\tag{17}
$$

Proof. Let $\eta = u - \mathcal{I}_h u$ and $e_h = u_h - \mathcal{I}_h u \in \mathcal{V}_1$, where $\mathcal{I}_h u$ is the interpolant of u in $\mathcal{V}_1$ with the approximation property (2). Firstly, we consider the case of $\|\boldsymbol{a}\| \geq \sigma h$. By virtue of the coercivity estimate (9) and the orthogonality property (10), we have

$$
\varepsilon\|\nabla e_h\|_0^2 + \frac{\sigma^2 h^2(\xi_1 - 1) + 8\sigma\varepsilon + 2\sigma\|\boldsymbol{a}\|h}{\sigma h^2 \xi_1 + 8\varepsilon + 2\|\boldsymbol{a}\|h}\|e_h\|_0^2 + \frac{h^2}{\sigma h^2 \xi_1 + 8\varepsilon + 2\|\boldsymbol{a}\|h}\|\boldsymbol{a}\cdot\nabla e_h\|_0^2
$$

$$
= B(e_h, e_h) = B(u_h - \mathcal{I}_h u, e_h) = B(u - \mathcal{I}_h u + u_h - u, e_h)
$$

$$
= B(\eta, e_h)
$$

$$
= \varepsilon(\nabla\eta, \nabla e_h)_0 + (\boldsymbol{a}\cdot\nabla\eta, e_h)_0 + \sigma(\eta, e_h)_0 - \sum_{T\in\mathcal{T}_h} \frac{h^2}{\sigma h^2 \xi_1 + 8\varepsilon + 2\|\boldsymbol{a}\|h}\left(-\varepsilon\Delta u + \boldsymbol{a}\cdot\nabla\eta + \sigma\eta,\; -\frac{\boldsymbol{a}\cdot\nabla e_h}{\gamma} + \sigma e_h\right)_{0,T}
$$

$$
= \varepsilon(\nabla\eta, \nabla e_h)_0 + \frac{\sigma h^2(\xi_1 - 1) + 8\varepsilon + 2\|\boldsymbol{a}\|h}{\sigma h^2 \xi_1 + 8\varepsilon + 2\|\boldsymbol{a}\|h}(\boldsymbol{a}\cdot\nabla\eta, e_h)_0 + \frac{\sigma^2 h^2(\xi_1 - 1) + 8\sigma\varepsilon + 2\sigma\|\boldsymbol{a}\|h}{\sigma h^2 \xi_1 + 8\varepsilon + 2\|\boldsymbol{a}\|h}(\eta, e_h)_0
$$

$$
+ \frac{h^2\varepsilon\sigma}{\sigma h^2 \xi_1 + 8\varepsilon + 2\|\boldsymbol{a}\|h}(\Delta u, e_h)_0 + \frac{h^2}{\sigma h^2 \xi_1 + 8\varepsilon + 2\|\boldsymbol{a}\|h}\left(-\varepsilon\Delta u + \boldsymbol{a}\cdot\nabla\eta + \sigma\eta,\; \frac{\boldsymbol{a}\cdot\nabla e_h}{\gamma}\right)_0
$$

$$
:= I_1 + I_2 + I_3 + I_4 + I_5,
$$

where note that $\gamma = 1$ from (7). We now estimate each term I_i as follows. Assume that $\sigma > 0$. Let α be a positive number that will be determined later. Then from Hölder's inequality and Young's inequality with Green's formula, we have

$$
I_1 \leq \varepsilon\left(\alpha\|\nabla e_h\|_0^2 + \frac{1}{\alpha}\|\nabla\eta\|_0^2\right),
$$

$$
I_2 = -\frac{\sigma h^2(\xi_1 - 1) + 8\varepsilon + 2\|\boldsymbol{a}\|h}{\sigma h^2 \xi_1 + 8\varepsilon + 2\|\boldsymbol{a}\|h}(\eta, \boldsymbol{a}\cdot\nabla e_h)_0
$$

$$
\leq \frac{h^2}{\sigma h^2 \xi_1 + 8\varepsilon + 2\|\boldsymbol{a}\|h}\alpha\|\boldsymbol{a}\cdot\nabla e_h\|_0^2 + \frac{(\sigma h^2(\xi_1 - 1) + 8\varepsilon + 2\|\boldsymbol{a}\|h)^2}{(\sigma h^2 \xi_1 + 8\varepsilon + 2\|\boldsymbol{a}\|h)h^2}\frac{1}{\alpha}\|\eta\|_0^2,
$$

$$
I_3 \leq \frac{\sigma^2 h^2(\xi_1 - 1) + 8\sigma\varepsilon + 2\sigma\|\boldsymbol{a}\|h}{\sigma h^2 \xi_1 + 8\varepsilon + 2\|\boldsymbol{a}\|h}\left(\alpha\|e_h\|_0^2 + \frac{1}{\alpha}\|\eta\|_0^2\right),
$$

$$
I_4 \leq \frac{\sigma^2 h^2(\xi_1 - 1) + 8\sigma\varepsilon + 2\sigma\|\boldsymbol{a}\|h}{\sigma h^2 \xi_1 + 8\varepsilon + 2\|\boldsymbol{a}\|h}\alpha\|e_h\|_0^2 + \frac{h^4\varepsilon^2\sigma^2}{(\sigma h^2 \xi_1 + 8\varepsilon + 2\|\boldsymbol{a}\|h)(\sigma^2 h^2(\xi_1 - 1) + 8\sigma\varepsilon + 2\sigma\|\boldsymbol{a}\|h)}\frac{1}{\alpha}\|\Delta u\|_0^2,
$$

$$
I_5 \leq \frac{h^2}{\sigma h^2 \xi_1 + 8\varepsilon + 2\|\boldsymbol{a}\|h}\left(3\alpha\|\boldsymbol{a}\cdot\nabla e_h\|_0^2 + \frac{1}{\alpha}\left(\varepsilon^2\|\Delta u\|_0^2 + \|\boldsymbol{a}\cdot\nabla\eta\|_0^2 + \sigma^2\|\eta\|_0^2\right)\right).
$$

Taking $\alpha = 1/5$ with the approximation property (2), we obtain

$$
\varepsilon \|\nabla e_h\|_0^2 + \frac{\sigma^2 h^2 (\xi_1 - 1) + 8\sigma\varepsilon + 2\sigma\|\boldsymbol{a}\|h}{\sigma h^2 \xi_1 + 8\varepsilon + 2\|\boldsymbol{a}\|h} \|e_h\|_0^2 + \frac{h^2}{\sigma h^2 \xi_1 + 8\varepsilon + 2\|\boldsymbol{a}\|h} \|\boldsymbol{a} \cdot \nabla e_h\|_0^2
$$

$$
\leq C \Bigg\{ \varepsilon \|\nabla \eta\|_0^2 + \frac{\big(\sigma h^2 (\xi_1 - 1) + 8\varepsilon + 2\|\boldsymbol{a}\|h\big)^2}{\big(\sigma h^2 \xi_1 + 8\varepsilon + 2\|\boldsymbol{a}\|h\big) h^2} \|\eta\|_0^2 + \frac{\sigma^2 h^2 (\xi_1 - 1) + 8\sigma\varepsilon + 2\sigma\|\boldsymbol{a}\|h}{\sigma h^2 \xi_1 + 8\varepsilon + 2\|\boldsymbol{a}\|h} \|\eta\|_0^2
$$

$$
+ \frac{h^4 \varepsilon^2 \sigma^2}{\big(\sigma h^2 \xi_1 + 8\varepsilon + 2\|\boldsymbol{a}\|h\big)\big(\sigma^2 h^2 (\xi_1 - 1) + 8\sigma\varepsilon + 2\sigma\|\boldsymbol{a}\|h\big)} \|\Delta u\|_0^2
$$

$$
+ \frac{h^2}{\sigma h^2 \xi_1 + 8\varepsilon + 2\|\boldsymbol{a}\|h} \big(\varepsilon^2 \|\Delta u\|_0^2 + \|\boldsymbol{a} \cdot \nabla \eta\|_0^2 + \sigma^2 \|\eta\|_0^2\big) \Bigg\}
$$

$$
\leq C \Bigg\{ \varepsilon h^2 + \frac{\big(\sigma h^2 (\xi_1 - 1) + 8\varepsilon + 2\|\boldsymbol{a}\|h\big)^2}{\big(\sigma h^2 \xi_1 + 8\varepsilon + 2\|\boldsymbol{a}\|h\big) h^2} h^4 + \frac{\sigma^2 h^2 (\xi_1 - 1) + 8\sigma\varepsilon + 2\sigma\|\boldsymbol{a}\|h}{\sigma h^2 \xi_1 + 8\varepsilon + 2\|\boldsymbol{a}\|h} h^4
$$

$$
+ \frac{h^4 \varepsilon^2 \sigma^2}{\big(\sigma h^2 \xi_1 + 8\varepsilon + 2\|\boldsymbol{a}\|h\big)\big(\sigma^2 h^2 (\xi_1 - 1) + 8\sigma\varepsilon + 2\sigma\|\boldsymbol{a}\|h\big)}
$$

$$
+ \frac{h^2}{\sigma h^2 \xi_1 + 8\varepsilon + 2\|\boldsymbol{a}\|h} \big(\varepsilon^2 + \|\boldsymbol{a}\|^2 h^2 + \sigma^2 h^4\big) \Bigg\} \|u\|_2^2, \tag{18}
$$

which implies

$$
\|\nabla e_h\|_0^2 \leq C \left(h^2 + \frac{\|\boldsymbol{a}\|}{\varepsilon} h^3 + \frac{\sigma}{\varepsilon} h^4 \right) \|u\|_2^2 \leq C \left(h^2 + \frac{\|\boldsymbol{a}\|}{\varepsilon} h^3 \right) \|u\|_2^2 \qquad \text{if } \|\boldsymbol{a}\| \geq \sigma h > 0. \tag{19}
$$

Now, combining the triangle inequality

$$
\|\nabla u - \nabla u_h\|_0 \leq \|\nabla u - \nabla(\mathcal{I}_h u)\|_0 + \|\nabla e_h\|_0
$$

with (19) and the interpolation property (2), we complete the proof of the first part of (16) for $\|\boldsymbol{a}\| \geq \sigma h > 0$. We remark that for the case of $\sigma = 0$, one can check that the first part of (16) still holds since $I_4 = 0$ and then the proof can be further simplified.

Secondly, we consider the other case, $\|\boldsymbol{a}\| < \sigma h$. Again, utilizing the coercivity estimate (9) and the orthogonality property (10), we have

$$
\varepsilon \|\nabla e_h\|_0^2 + \frac{\sigma^2 h^2 (\xi_1 - 1) + 8\sigma\varepsilon}{\sigma h^2 \xi_1 + 8\varepsilon + 2\|\boldsymbol{a}\|h} \|e_h\|_0^2 + \frac{h^2 + 2\|\boldsymbol{a}\|h/\sigma}{(\sigma h^2 \xi_1 + 8\varepsilon + 2\|\boldsymbol{a}\|h)\gamma} \|\boldsymbol{a} \cdot \nabla e_h\|_0^2
$$

$$
= B(e_h, e_h) = B(u_h - \mathcal{I}_h u, e_h) = B(u - \mathcal{I}_h u + u_h - u, e_h)
$$

$$
= B(\eta, e_h)
$$

$$
= \varepsilon (\nabla \eta, \nabla e_h)_0 + (\boldsymbol{a} \cdot \nabla \eta, e_h)_0 + \sigma(\eta, e_h)_0
$$

$$
- \sum_{T \in \mathcal{T}_h} \frac{h^2 + 2\|\boldsymbol{a}\|h/\sigma}{\sigma h^2 \xi_1 + 8\varepsilon + 2\|\boldsymbol{a}\|h} \left(-\varepsilon \Delta u + \boldsymbol{a} \cdot \nabla \eta + \sigma \eta, -\frac{\boldsymbol{a} \cdot \nabla e_h}{\gamma} + \sigma e_h \right)_{0,T}
$$

$$
= \varepsilon (\nabla \eta, \nabla e_h)_0 + \frac{\sigma h^2 (\xi_1 - 1) + 8\varepsilon}{\sigma h^2 \xi_1 + 8\varepsilon + 2\|\boldsymbol{a}\|h} (\boldsymbol{a} \cdot \nabla \eta, e_h)_0 + \frac{\sigma^2 h^2 (\xi_1 - 1) + 8\sigma\varepsilon}{\sigma h^2 \xi_1 + 8\varepsilon + 2\|\boldsymbol{a}\|h} (\eta, e_h)_0
$$

$$
+ \frac{h^2 + 2\|\boldsymbol{a}\|h/\sigma}{\sigma h^2 \xi_1 + 8\varepsilon + 2\|\boldsymbol{a}\|h} \varepsilon \sigma (\Delta u, e_h)_0 + \frac{h^2 + 2\|\boldsymbol{a}\|h/\sigma}{(\sigma h^2 \xi_1 + 8\varepsilon + 2\|\boldsymbol{a}\|h)\gamma} (-\varepsilon \Delta u + \boldsymbol{a} \cdot \nabla \eta + \sigma \eta, \boldsymbol{a} \cdot \nabla e_h)_0
$$

$$
:= J_1 + J_2 + J_3 + J_4 + J_5.
$$

Similar to the treatment of above case, we estimate each term J_i as follows. Let β be a positive number that will be determined later. By virtue of Hölder's inequality and Young's inequality with the definition (7) of the parameter γ, we have the following estimates:

$$
J_1 \leq \varepsilon\left(\beta\|\nabla e_h\|_0^2 + \frac{1}{\beta}\|\nabla\eta\|_0^2\right),
$$

$$
J_2 \leq \frac{\sigma h^2(\xi_1 - 1) + 8\varepsilon}{\sigma h^2\xi_1 + 8\varepsilon + 2\|\boldsymbol{a}\|h}\left(\beta\sigma\|e_h\|_0^2 + \frac{1}{\beta\sigma}\|\boldsymbol{a}\cdot\nabla\eta\|_0^2\right),
$$

$$
J_3 \leq \frac{\sigma^2 h^2(\xi_1 - 1) + 8\sigma\varepsilon}{\sigma h^2\xi_1 + 8\varepsilon + 2\|\boldsymbol{a}\|h}\left(\beta\|e_h\|_0^2 + \frac{1}{\beta}\|\eta\|_0^2\right),
$$

$$
J_4 \leq \frac{\sigma^2 h^2(\xi_1 - 1) + 8\sigma\varepsilon}{\sigma h^2\xi_1 + 8\varepsilon + 2\|\boldsymbol{a}\|h}\beta\|e_h\|_0^2 + \frac{\left(h^2 + 2\|\boldsymbol{a}\|h/\sigma\right)\left(h^2 + 2\|\boldsymbol{a}\|h/\sigma\right)\varepsilon^2\sigma^2}{\left(\sigma h^2\xi_1 + 8\varepsilon + 2\|\boldsymbol{a}\|h\right)\left(\sigma^2 h^2(\xi_1 - 1) + 8\sigma\varepsilon\right)}\frac{1}{\beta}\|\Delta u\|_0^2,
$$

$$
J_5 \leq \frac{h^2 + 2\|\boldsymbol{a}\|h/\sigma}{(\sigma h^2\xi_1 + 8\varepsilon + 2\|\boldsymbol{a}\|h)\gamma}\left(3\beta\|\boldsymbol{a}\cdot\nabla e_h\|_0^2 + \frac{1}{\beta}\left(\varepsilon^2\|\Delta u\|_0^2 + \|\boldsymbol{a}\cdot\nabla\eta\|_0^2 + \sigma^2\|\eta\|_0^2\right)\right)
$$

$$
\leq \frac{h^2 + 2\|\boldsymbol{a}\|h/\sigma}{(\sigma h^2\xi_1 + 8\varepsilon + 2\|\boldsymbol{a}\|h)\gamma}3\beta\|\boldsymbol{a}\cdot\nabla e_h\|_0^2 + \frac{\left(h^2 + 2\|\boldsymbol{a}\|h/\sigma\right)\left(h^2 + 2\|\boldsymbol{a}\|_2 h/\sigma\right)\varepsilon^2\sigma^2}{\left(\sigma h^2\xi_1 + 8\varepsilon + 2\|\boldsymbol{a}\|h\right)\left(\sigma^2 h^2(\xi_1 - 1) + 8\sigma\varepsilon\right)}\left(\frac{1}{\beta}\right)\|\Delta u\|_0^2
$$

$$
+ \frac{h^2(\xi_1 - 1) + 8\varepsilon/\sigma}{\sigma h^2\xi_1 + 8\varepsilon + 2\|\boldsymbol{a}\|h}\left(\frac{1}{\beta}\right)\|\boldsymbol{a}\cdot\nabla\eta\|_0^2 + \frac{\sigma^2 h^2(\xi_1 - 1) + 8\sigma\varepsilon}{\sigma h^2\xi_1 + 8\varepsilon + 2\|\boldsymbol{a}\|h}\left(\frac{1}{\beta}\right)\|\eta\|_0^2.
$$

Taking $\beta = 1/4$ with the interpolation property (2), we obtain

$$
\varepsilon\|\nabla e_h\|_0^2 + \frac{\sigma^2 h^2(\xi_1 - 1) + 8\sigma\varepsilon}{\sigma h^2\xi_1 + 8\varepsilon + 2\|\boldsymbol{a}\|h}\|e_h\|_0^2 + \frac{h^2 + 2\|\boldsymbol{a}\|h/\sigma}{(\sigma h_T^2\xi_1 + 8\varepsilon + 2\|\boldsymbol{a}\|h)\gamma}\|\boldsymbol{a}\cdot\nabla e_h\|_0^2
$$

$$
\leq C\Bigg\{\varepsilon\|\nabla\eta\|_0^2 + \frac{h^2(\xi_1 - 1) + 8\varepsilon/\sigma}{\sigma h^2\xi_1 + 8\varepsilon + 2\|\boldsymbol{a}\|h}\|\boldsymbol{a}\|^2\|\nabla\eta\|_0^2 + \frac{\sigma^2 h^2(\xi_1 - 1) + 8\sigma\varepsilon}{\sigma h^2\xi_1 + 8\varepsilon + 2\|\boldsymbol{a}\|h}\|\eta\|_0^2
$$

$$
+ \frac{\left(h^2 + 2\|\boldsymbol{a}\|h/\sigma\right)\left(h^2 + 2\|\boldsymbol{a}\|h/\sigma\right)\varepsilon^2\sigma^2}{\left(\sigma h^2\xi_1 + 8\varepsilon + 2\|\boldsymbol{a}\|h\right)\left(\sigma^2 h^2(\xi_1 - 1) + 8\sigma\varepsilon\right)}\|\Delta u\|_0^2\Bigg\}
$$

$$
\leq C\Bigg\{\varepsilon h^2 + \frac{h^2(\xi_1 - 1) + 8\varepsilon/\sigma}{\sigma h^2\xi_1 + 8\varepsilon + 2\|\boldsymbol{a}\|h}\|\boldsymbol{a}\|^2 h^2 + \frac{\sigma^2 h^2(\xi_1 - 1) + 8\sigma\varepsilon}{\sigma h^2\xi_1 + 8\varepsilon + 2\|\boldsymbol{a}\|h}h^4
$$

$$
+ \frac{\left(h^2 + 2\|\boldsymbol{a}\|h/\sigma\right)\left(h^2 + 2\|\boldsymbol{a}\|h/\sigma\right)\varepsilon^2\sigma^2}{\left(\sigma h^2\xi_1 + 8\varepsilon + 2\|\boldsymbol{a}\|h\right)\left(\sigma^2 h^2(\xi_1 - 1) + 8\sigma\varepsilon\right)}\Bigg\}\|u\|_2^2,
$$

which implies

$$
\|\nabla e_h\|_0^2 \leq C\left(h^2 + \frac{\|\boldsymbol{a}\|}{\sigma}h\right)\|u\|_2^2 \leq Ch^2\|u\|_2^2 \qquad \text{if } \|\boldsymbol{a}\| < \sigma h, \tag{20}
$$

$$
\|e_h\|_0^2 \leq C\left(h^4 + \frac{\|\boldsymbol{a}\|}{\sigma}h^3 + \frac{\|\boldsymbol{a}\|^2}{\sigma^2}h^2 + \frac{\varepsilon}{\sigma}h^2\right)\|u\|_2^2 \leq C\left(h^4 + \frac{\varepsilon}{\sigma}h^2\right)\|u\|_2^2 \qquad \text{if } \|\boldsymbol{a}\| < \sigma h. \tag{21}
$$

Finally, combining the triangle inequality with (20), (21) and the interpolation property (2) yields the conclusion. This completes the proof. $\square$

Remark 3. We define the mesh Péclet number as $Pe_h := \|\boldsymbol{a}\|h/(2\varepsilon)$ and the mesh Damköhler number as $Da_h := \sigma h/\|\boldsymbol{a}\|$. Theorem 2 shows that if $Pe_h > 1/2$ and $Da_h > 1$, then the second part of (16) and (17) can be respectively

9

rewritten as

$$\|\nabla u - \nabla u_h\|_0 \quad \leq \quad Ch\|u\|_2 \qquad \text{if } Da_h > 1, \tag{22}$$

$$\|u - u_h\|_0 \quad \leq \quad Ch^2\|u\|_2 \qquad \text{if } Da_h > 1 \text{ and } 2Pe_h > 1, \tag{23}$$

which indicates that the proposed stabilized linear FEM (3) achieves optimal convergence rates in H^1 norm and also in L^2 norm without using the duality argument, with respect to the mesh size h as well as the regularity of the exact solution $u \in H^2(\Omega)$. On the other hand, for a small mesh Damköhler number $Da_h \leq 1$, the errors of the stabilized finite element solutions generated by the proposed method behave like the well-known streamline upwind/Petrov-Galerkin formulation of Brooks and Hughes [6]. More precisely, from the first part of (16) we have

$$\|\nabla u - \nabla u_h\|_0 \leq C\left(h + h^{3/2}\sqrt{\frac{\|\boldsymbol{a}\|}{\varepsilon}}\right)\|u\|_2 \qquad \text{if } Da_h \leq 1. \tag{24}$$

Remark 4. With a close inspection of (18) in the proof of Theorem 2, we can also prove that

$$\|e_h\|_0^2 \leq C\left(h^4 + \frac{\varepsilon}{\sigma}h^2 + \frac{\|\boldsymbol{a}\|}{\sigma}h^3 + \frac{\sigma}{\|\boldsymbol{a}\|}h^5\right)\|u\|_2^2 \leq C\left(h^4 + \frac{\varepsilon}{\sigma}h^2 + \frac{\|\boldsymbol{a}\|}{\sigma}h^3\right)\|u\|_2^2 \qquad \text{if } \|\boldsymbol{a}\| \geq \sigma h > 0.$$

Using the triangle inequality,

$$\|u - u_h\|_0 \leq \|u - \mathcal{I}_h u\|_0 + \|e_h\|_0,$$

and the interpolation property (2), we obtain

$$\|u - u_h\|_0 \leq C\left(h^2 + h\sqrt{\frac{\varepsilon + \|\boldsymbol{a}\|h}{\sigma}}\right)\|u\|_2 \qquad \text{if } \|\boldsymbol{a}\| \geq \sigma h > 0. \tag{25}$$

Now, using the Poincaré-Friedrichs inequality and putting (24) and (25) together leads to

$$\|u - u_h\|_0 \leq C \min\left\{h + h^{3/2}\sqrt{\frac{\|\boldsymbol{a}\|}{\varepsilon}}, \quad h^2 + h\sqrt{\frac{\varepsilon + \|\boldsymbol{a}\|h}{\sigma}}\right\}\|u\|_2 \qquad \text{if } \|\boldsymbol{a}\| \geq \sigma h > 0. \tag{26}$$

This indicates that when $0 < \sigma h \leq \|\boldsymbol{a}\|$, the behavior of the L^2 errors is determined by the comparisons among the diffusivity ε, the reaction coefficient σ, and the modulus of the convection field $\|\boldsymbol{a}\|$.

4. Numerical experiments

In this section, we will perform numerical experiments to illustrate the obtained theoretical results. We will consider three test problems that are frequently used in the literature. The performance of the newly proposed stabilized linear FEM (3) will be evaluated against the results from the previous Duan-Hsieh-Tan-Yang method (14), which is briefly described in Remark 2 in Section 2. By comparison, we can find that the accuracy of both methods is comparable, while the newly proposed method (3) seems a little more stable than the previous method (14).

Example 1. This example is taken from [22]. We will study the convergence behavior of the proposed stabilized linear FEM (3) by a problem with an exact solution. Let $\Omega = (0,1) \times (0,1)$ and the convection field $\boldsymbol{a} = (a_1, a_2)^\top = (1/2, \sqrt{3}/2)^\top$. We assume that the exact solution u of problem (1) is given by

$$u(x,y) = \left(\frac{x^2}{2a_1} + \frac{\varepsilon x}{a_1^2} + \left(\frac{1}{2a_1} + \frac{\varepsilon}{a_1^2}\right)\frac{e^{\frac{-a_1}{\varepsilon}} - e^{\frac{-a_1}{\varepsilon}(1-x)}}{1 - e^{\frac{-a_1}{\varepsilon}}}\right)\left(\frac{y^2}{2a_2} + \frac{\varepsilon y}{a_2^2} + \left(\frac{1}{2a_2} + \frac{\varepsilon}{a_2^2}\right)\frac{e^{\frac{-a_2}{\varepsilon}} - e^{\frac{-a_2}{\varepsilon}(1-y)}}{1 - e^{\frac{-a_2}{\varepsilon}}}\right).$$

Substituting the solution u into problem (1) with various ε and σ, we can obtain the source function f. Notice that the solution is dependent on the diffusivity ε while it is independent of the reaction coefficient σ, and when the diffusivity ε is getting small, a strong boundary layer appears near the right up corner; see Figure 1.
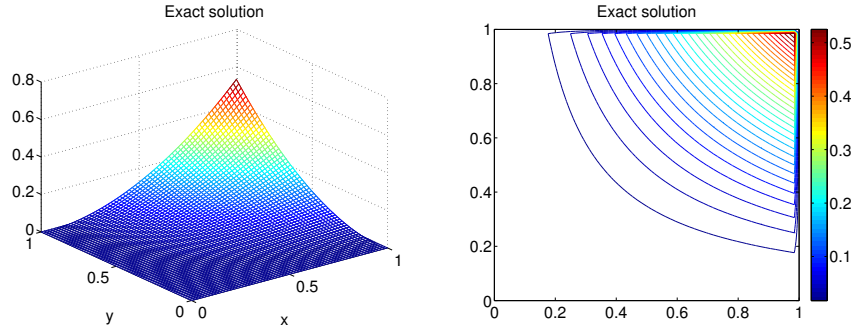
Figure 1. Elevation and contours of the exact solution u of Example 1 with $\varepsilon = 10^{-4}$.

We consider the stabilized linear finite element approximations to the problem on uniform square meshes and uniform triangular meshes. A uniform triangular mesh is formed by dividing each square, with side-length h^* in a uniform square mesh, into two triangles by drawing a diagonal line from the left-down corner to the right-up corner. In the computations, we use the continuous piecewise P_1 elements for uniform triangular meshes while the continuous piecewise Q_1 elements for uniform square meshes. We consider the values of $\varepsilon = 1, 0.1, 0.01$, $\sigma = 10^{\ell}$ for $\ell = -2, -1, \cdots, 4$ and compare the error behavior of the solutions generated by the new stabilized FEM (3) and the Duan-Hsieh-Tan-Yang method (14). It is worth to point out that, under the presence of convection, $\boldsymbol{a} \not\equiv \boldsymbol{0}$, a better choice of the element parameter h to yield better numerical results is defined as the largest diameter of element in the direction of $\boldsymbol{a}$; see [19]. Thus, in this example, we take the mesh parameter as $h = \sqrt{4/3}h^*$, since $\boldsymbol{a} = (1/2, \sqrt{3}/2)^{\top}$. The numerical raw data for P_1 elements are reported in Table 1 and Table 2, from which we may observe that the asymptotic convergence orders of both stabilized linear FEMs (3) and (14) are optimal in H^1 norm and L^2 norm. Moreover, the accuracy of the numerical results of both methods is comparable, while the present stabilized linear FEM (3) seems more suitable for problems with a larger mesh Péclet number and a larger mesh Damköhler number. This observation is consistent with the error estimates (22) and (23).

Next, we consider the smaller diffusivity $\varepsilon = 10^{-4}$. In this case, a strong boundary layer appears near the upper right corner. Numerical results using Q_1 elements with $\sigma = 10^2, 10^3, 10^4$, $h^* = 1/64$ and $h = \sqrt{4/3}h^*$ are displayed in Figure 2. From the numerical results, we may observe that when σ is not too large, say $\sigma = 10^2$, a little bit of oscillation still occurs near the boundary layer region in approximate solution produced by the Duan-Hsieh-Tan-Yang stabilized FEM and this spurious oscillation can not be eliminated even if we use a finer mesh such as $h = 1/128$. When σ is rather large, say $\sigma = 10^4$, the present stabilized FEM (3) gives stable results and it is able to capture the boundary layer behavior very well.

We now compare the performance of these two stabilization methods (3) and (14) for the computations on a given unstructured and adaptive mesh drawn in Figure 3. We use the stabilization parameters that are defined in Remark

11

1 for the method (3) while for method (14), we use the elementwise stabilization parameter given in (15) in Remark 2. The numerical results are depicted in Figure 4, from which we can find that the newly proposed stabilized linear FEM (3) can work very well, while the Duan-Hsieh-Tan-Yang stabilized FEM (14) seems a little unstable for such an adaptive mesh because the approximate solution oscillates slightly around the boundary layer region.
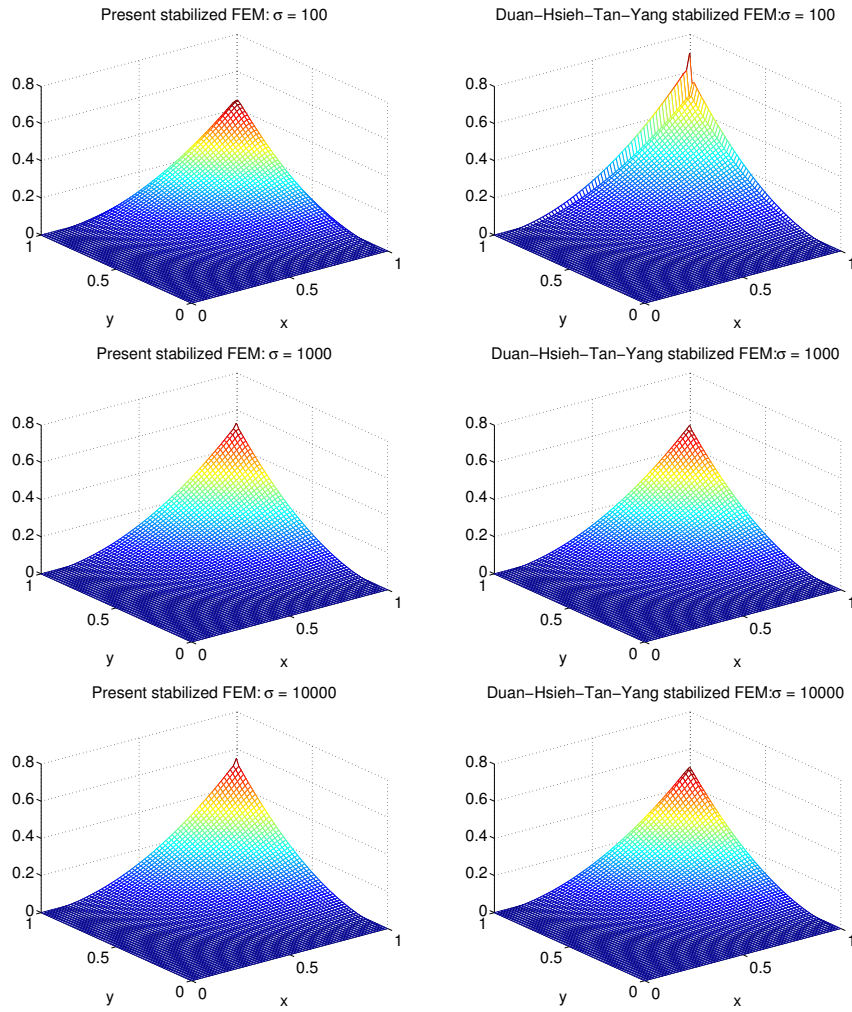
Figure 2. Elevation plots of the stabilized finite element solutions of Example 1 with $\varepsilon = 10^{-4}$ and $\sigma = 10^2, 10^3, 10^4$, using Q_1 elements, $h^* = 1/64$ and $h = \sqrt{4/3}h^*$.

Table 1. L^2 relative errors of u_h using P_1 elements for Example 1 with various ε and σ.

L^2-error	ε	σ	$h^* = 1/32$	$h^* = 1/64$	$h^* = 1/128$	$h^* = 1/256$	order $\approx$
Present method	1	10^{-2}	3.0923E-03	7.7405E-04	1.9358E-04	4.8399E-05	2.00
		10^{-1}	3.0900E-03	7.7347E-04	1.9343E-04	4.8363E-05	2.00
		10^{0}	3.0674E-03	7.6782E-04	1.9202E-04	4.8010E-05	2.00
		10^{1}	2.9068E-03	7.2749E-04	1.8194E-04	4.5491E-05	2.00
		10^{2}	3.2508E-03	9.9898E-04	1.5849E-04	3.9624E-05	2.00
		10^{3}	2.6011E-03	6.4309E-04	1.7080E-04	4.8646E-05	1.81
		10^{4}	4.1933E-03	6.9976E-04	1.5272E-04	3.7625E-05	2.02
Present method	0.1	10^{-2}	7.0191E-03	1.7729E-03	4.4510E-04	1.1149E-04	2.00
		10^{-1}	7.0225E-03	1.7737E-03	4.4531E-04	1.1154E-04	2.00
		10^{0}	7.0432E-03	1.7787E-03	4.4658E-04	1.1186E-04	2.00
		10^{1}	6.9569E-03	1.7545E-03	4.4049E-04	1.1036E-04	2.00
		10^{2}	9.0559E-03	2.7270E-03	4.1913E-04	1.0489E-04	2.00
		10^{3}	1.1634E-02	2.1061E-03	4.9517E-04	1.3732E-04	1.85
		10^{4}	1.1277E-02	2.9403E-03	7.5546E-04	1.1813E-04	2.68
Present method	0.01	10^{-2}	9.0582E-02	2.8545E-02	7.8174E-03	2.0241E-03	1.95
		10^{-1}	9.0608E-02	2.8548E-02	7.8179E-03	2.0242E-03	1.95
		10^{0}	9.0863E-02	2.8583E-02	7.8223E-03	2.0248E-03	1.95
		10^{1}	9.2990E-02	2.8839E-02	7.8490E-03	2.0278E-03	1.95
		10^{2}	1.4326E-01	4.4905E-02	7.9414E-03	2.0263E-03	1.97
		10^{3}	1.1782E-01	4.2598E-02	1.3993E-02	2.7109E-03	2.37
		10^{4}	1.1594E-01	4.0718E-02	1.2416E-02	3.4998E-03	1.83
Duan-Hsieh-Tan-Yang method	1	10^{-2}	2.9762E-03	7.4488E-04	1.8627E-04	4.6571E-05	2.00
		10^{-1}	2.9838E-03	7.4679E-04	1.8675E-04	4.6691E-05	2.00
		10^{0}	3.0576E-03	7.6525E-04	1.9137E-04	4.7845E-05	2.00
		10^{1}	3.5937E-03	8.9951E-04	2.2494E-04	5.6240E-05	2.00
		10^{2}	4.7609E-03	1.1926E-03	2.9830E-04	7.4584E-05	2.00
		10^{3}	5.3168E-03	1.3349E-03	3.3408E-04	8.3544E-05	2.00
		10^{4}	5.4468E-03	1.3728E-03	3.4409E-04	8.6085E-05	2.00
Duan-Hsieh-Tan-Yang method	0.1	10^{-2}	5.7654E-03	1.4456E-03	3.6167E-04	9.0432E-05	2.00
		10^{-1}	5.7820E-03	1.4499E-03	3.6273E-04	9.0699E-05	2.00
		10^{0}	6.0577E-03	1.5195E-03	3.8017E-04	9.5062E-05	2.00
		10^{1}	8.8649E-03	2.2283E-03	5.5783E-04	1.3950E-04	2.00
		10^{2}	1.2720E-02	3.2364E-03	8.1285E-04	2.0345E-04	2.00
		10^{3}	1.4118E-02	3.6739E-03	9.3110E-04	2.3367E-04	1.99
		10^{4}	1.4349E-02	3.7761E-03	9.6679E-04	2.4397E-04	1.99
Duan-Hsieh-Tan-Yang method	0.01	10^{-2}	8.4636E-02	2.4046E-02	6.2483E-03	1.5779E-03	1.99
		10^{-1}	8.4517E-02	2.4036E-02	6.2472E-03	1.5777E-03	1.99
		10^{0}	8.3535E-02	2.3971E-02	6.2440E-03	1.5778E-03	1.98
		10^{1}	8.4915E-02	2.5222E-02	6.6365E-03	1.6813E-03	1.98
		10^{2}	1.1518E-01	3.7618E-02	1.0364E-02	2.6640E-03	1.96
		10^{3}	1.2741E-01	4.6096E-02	1.4102E-02	3.8459E-03	1.87
		10^{4}	1.2890E-01	4.7429E-02	1.4983E-02	4.2608E-03	1.81

Table 2. H^1 relative errors of u_h using P_1 elements for Example 1 with various ε and σ.

H^1-error	ε	σ	$h^* = 1/32$	$h^* = 1/64$	$h^* = 1/128$	$h^* = 1/256$	order $\approx$
Present method	1	10^{-2}	5.5816E-02	2.7927E-02	1.3966E-02	6.9832E-03	1.00
		10^{-1}	5.5816E-02	2.7927E-02	1.3966E-02	6.9832E-03	1.00
		10^{0}	5.5816E-02	2.7927E-02	1.3966E-02	6.9832E-03	1.00
		10^{1}	5.5816E-02	2.7927E-02	1.3966E-02	6.9832E-03	1.00
		10^{2}	5.5823E-02	2.7930E-02	1.3966E-02	6.9832E-03	1.00
		10^{3}	5.5853E-02	2.7932E-02	1.3966E-02	6.9833E-03	1.00
		10^{4}	5.6001E-02	2.7946E-02	1.3968E-02	6.9835E-03	1.00
Present method	0.1	10^{-2}	1.0641E-01	5.3402E-02	2.6726E-02	1.3366E-02	1.00
		10^{-1}	1.0641E-01	5.3402E-02	2.6726E-02	1.3366E-02	1.00
		10^{0}	1.0641E-01	5.3402E-02	2.6726E-02	1.3366E-02	1.00
		10^{1}	1.0641E-01	5.3402E-02	2.6726E-02	1.3366E-02	1.00
		10^{2}	1.0656E-01	5.3468E-02	2.6727E-02	1.3366E-02	1.00
		10^{3}	1.0752E-01	5.3452E-02	2.6732E-02	1.3368E-02	1.00
		10^{4}	1.0758E-01	5.3758E-02	2.6812E-02	1.3369E-02	1.00
Present method	0.01	10^{-2}	5.6192E-01	3.3331E-01	1.7622E-01	8.9463E-02	0.98
		10^{-1}	5.6190E-01	3.3331E-01	1.7622E-01	8.9463E-02	0.98
		10^{0}	5.6177E-01	3.3330E-01	1.7622E-01	8.9463E-02	0.98
		10^{1}	5.6083E-01	3.3323E-01	1.7622E-01	8.9462E-02	0.98
		10^{2}	5.7874E-01	3.4071E-01	1.7621E-01	8.9463E-02	0.98
		10^{3}	5.6478E-01	3.3985E-01	1.8109E-01	8.9674E-02	1.01
		10^{4}	5.6400E-01	3.3845E-01	1.7966E-01	9.0832E-02	0.98
Duan-Hsieh-Tan-Yang method	1	10^{-2}	5.5816E-02	2.7927E-02	1.3966E-02	6.9832E-03	1.00
		10^{-1}	5.5816E-02	2.7927E-02	1.3966E-02	6.9832E-03	1.00
		10^{0}	5.5816E-02	2.7927E-02	1.3966E-02	6.9832E-03	1.00
		10^{1}	5.5821E-02	2.7928E-02	1.3966E-02	6.9832E-03	1.00
		10^{2}	5.5871E-02	2.7934E-02	1.3967E-02	6.9833E-03	1.00
		10^{3}	5.6010E-02	2.7954E-02	1.3969E-02	6.9836E-03	1.00
		10^{4}	5.6181E-02	2.7997E-02	1.3977E-02	6.9846E-03	1.00
Duan-Hsieh-Tan-Yang method	0.1	10^{-2}	1.0656E-01	5.3421E-02	2.6728E-02	1.3367E-02	1.00
		10^{-1}	1.0655E-01	5.3420E-02	2.6728E-02	1.3367E-02	1.00
		10^{0}	1.0648E-01	5.3412E-02	2.6727E-02	1.3366E-02	1.00
		10^{1}	1.0647E-01	5.3410E-02	2.6727E-02	1.3366E-02	1.00
		10^{2}	1.0737E-01	5.3546E-02	2.6745E-02	1.3369E-02	1.00
		10^{3}	1.0875E-01	5.3928E-02	2.6811E-02	1.3378E-02	1.00
		10^{4}	1.0917E-01	5.4213E-02	2.6919E-02	1.3401E-02	1.01
Duan-Hsieh-Tan-Yang method	0.01	10^{-2}	6.0995E-01	3.4298E-01	1.7764E-01	8.9649E-02	0.99
		10^{-1}	6.0931E-01	3.4289E-01	1.7763E-01	8.9647E-02	0.99
		10^{0}	6.0343E-01	3.4203E-01	1.7752E-01	8.9633E-02	0.99
		10^{1}	5.7319E-01	3.3679E-01	1.7680E-01	8.9542E-02	0.98
		10^{2}	5.6373E-01	3.3533E-01	1.7677E-01	8.9550E-02	0.98
		10^{3}	5.7004E-01	3.4370E-01	1.8150E-01	9.0813E-02	1.00
		10^{4}	5.7098E-01	3.4561E-01	1.8382E-01	9.2342E-02	0.99
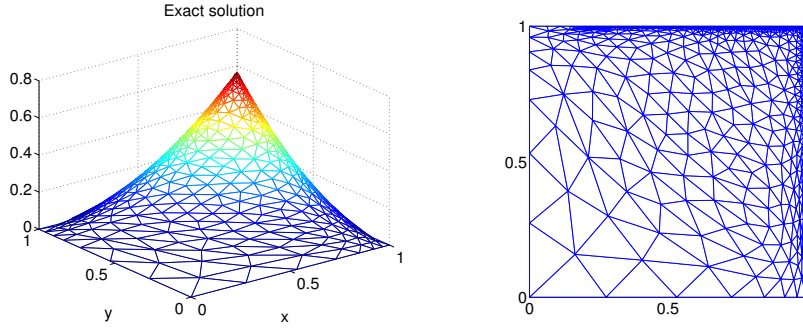
Figure 3. Elevation of the exact solution u of Example 1 with $\varepsilon = 10^{-4}$ on a given unstructured adaptive mesh containing 1509 triangles and 901 nodes.
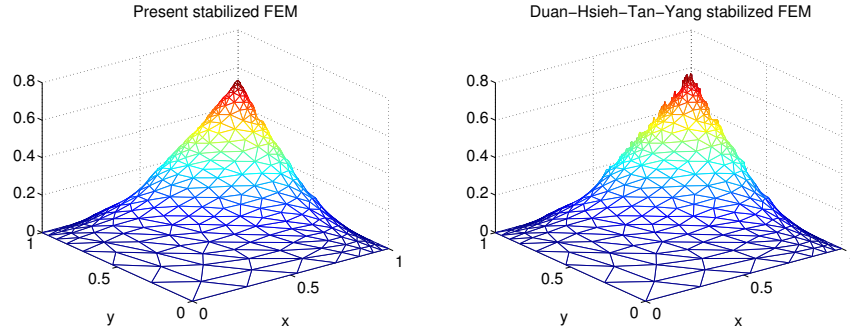
Figure 4. Elevation plots of the stabilized finite element solutions of Example 1 with $\varepsilon = 10^{-4}$ and $\sigma = 10^3$, using P_1 elements on the unstructured adaptive mesh given in Figure 3.

Example 2. This example is quoted from [19]. We will consider the reaction-convection-diffusion equation with $\varepsilon = 10^{-6}$, variable convection field $\boldsymbol{a}(x, y) = (2y, 0)^\top$, $\sigma = 10^4$ and $f = 0$ on the rectangular domain $\Omega = (0, 1) \times (0, 1/2)$ subject to the boundary conditions described in Figure 5. We wish to test the performance of the stabilized linear FEM (3) using P_1 elements on an unstructured mesh that is depicted in Figure 6. This mesh is constructed by dividing each side of the rectangle Ω into equal segments with length $h^* = 1/32$ and then using the *FreeFem++* (see [26]) to generate an unstructured quasi-uniform mesh. The elevation and contour plots for the approximate solutions u_h of the the present stabilized linear FEM (3) and the Duan-Hsieh-Tan-Yang stabilized linear FEM (14) are displayed in Figure 7, where we use the elementwise defined stabilization parameters as that described in Remark 1 and Remark 2 in Section 2. Although the exact solution of this problem is not available here, from the results reported in the literature [19], it is supposed that the solution shape should look like the shape of the approximate solution generated by the present stabilized FEM. One can also find from Figure 7 that the result of the present method (3) is comparable to that of the Duan-Hsieh-Tan-Yang method (14).
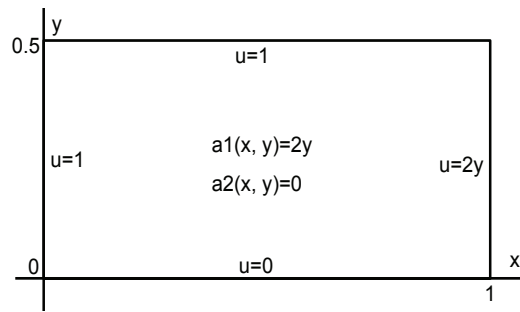
Figure 5. Boundary conditions and convection field of Example 2.
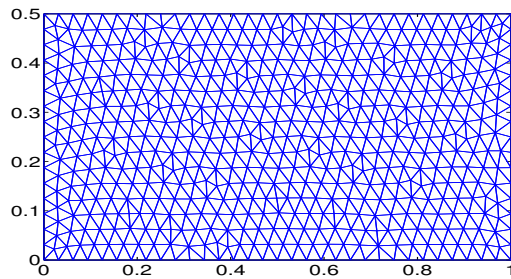
Figure 6. An unstructured mesh with $h^* = 1/32$ for Example 2.
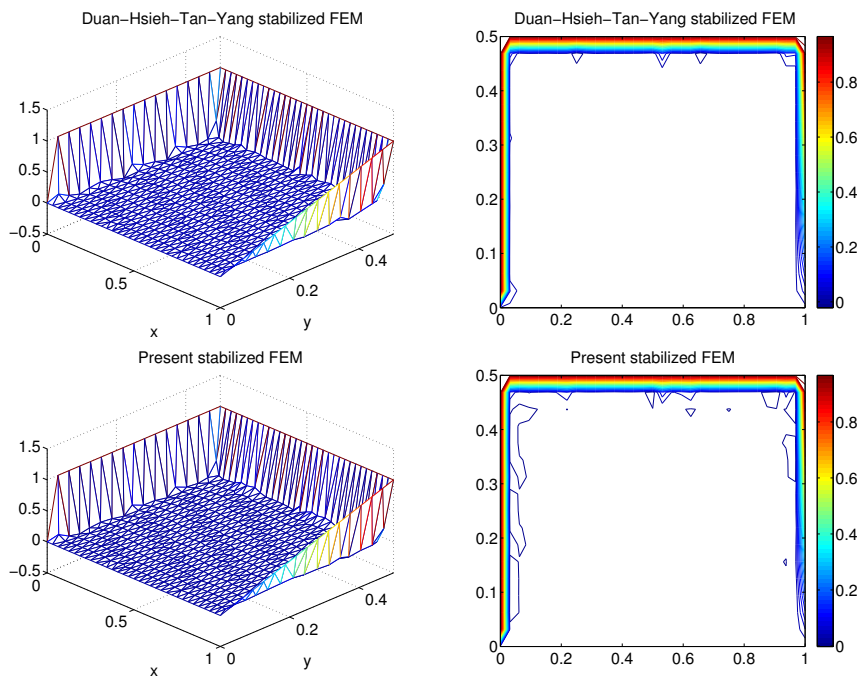
Figure 7. Elevation and contours of the stabilized finite element solutions of Example 2 with $\varepsilon = 10^{-6}$, $\sigma = 10^4$ and $\boldsymbol{a} = (2y, 0)^\top$, using P_1 elements on an unstructured mesh given in Figure 6 and $h^* = 1/32$.

Example 3. (cf. [19]) We now give an example to demonstrate that the proposed stabilized linear FEM (3) is suitable for all sizes of σ even if the diffusivity ε is small enough. We consider a problem with $f = 0$, $\varepsilon = 10^{-6}$, and impose

the boundary conditions described in Figure 8. The prescribed constant convection field is given by $\boldsymbol{a} = (0.15, 0.1)^{\top}$. We use Q_1 elements on uniform square meshes. The side-length of each square in a uniform square mesh is denoted by h^* and the mesh parameter is taken as $h = \sqrt{13/9}h^*$ which is the largest diameter of element in the direction of $\boldsymbol{a}$.
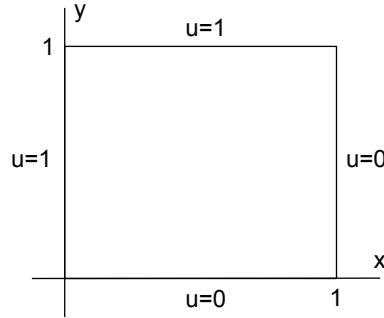
Figure 8. Boundary conditions of Example 3.

The elevation and contours of the approximate solutions for $h^* = 1/32$ and different values of reaction coefficient are displayed in Figure 9. Again, the exact solutions are not available here for various σ. However, from the results reported in the literature (cf. [19]), we believe that their shapes should look like the shapes of numerical solutions generated by the present stabilized FEM. From the numerical results, we can observe that for a problem with a given small diffusivity $\varepsilon = 10^{-6}$, the proposed stabilized linear FEM (3) always gives stable and accurate results and it is able to capture the behavior of boundary and interior layers, even we use a relatively coarse mesh with $h^* = 1/32$.
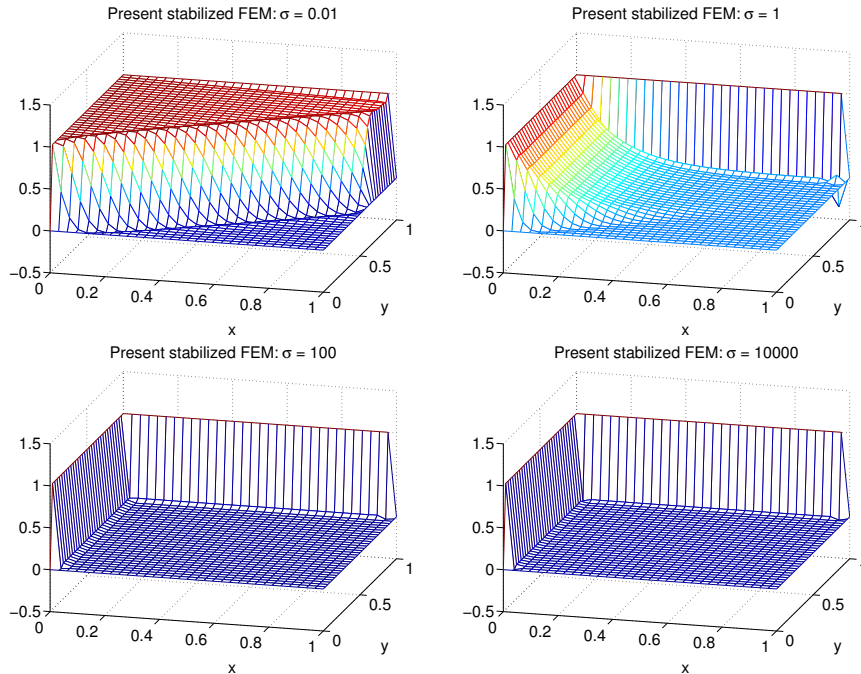
Figure 9. Elevation plots of the stabilized finite element solutions of Example 3 with $\varepsilon = 10^{-6}$, $\sigma = 10^{-2}, 1, 10^2, 10^4$ and $\boldsymbol{a} = (0.15, 0.1)^{\top}$, using Q_1 elements, $h^* = 1/32$ and $h = \sqrt{13/9}h^*$.

5. Application of the stabilization method to time-dependent reaction-convection-diffusion problems

In this section, with the help of the the stabilized linear FEM (3), we are going to propose a stabilization scheme for solving time-dependent reaction-convection-diffusion problems. Let $[0, T]$ be the time interval under consideration and Ω the given spatial domain. Consider the following initial-boundary value problem:

$$\begin{cases} \dfrac{\partial u}{\partial t} - \varepsilon \Delta u + \boldsymbol{a} \cdot \nabla u + \sigma u = & f & \text{in } (0, T] \times \Omega, \\ u(0, x, y) = & u_0(x, y) & \text{for } (x, y) \in \Omega, \\ u(t, x, y) = & 0 & \text{for } (x, y) \in \partial\Omega, \ 0 < t \le T. \end{cases} \tag{27}$$

Based on the stabilized linear FEM (3) for the steady-state problem (1), we first state the semi-discrete formulation of problem (27) as follows: Find $u_h(t, x, y) \in \mathcal{V}_1$ for $t \in (0, T]$ with $u_h(0, x, y) = u_0(x, y)$ such that

$$\left(\dfrac{\partial u_h}{\partial t}, v_h\right)_0 + \varepsilon(\nabla u_h, \nabla v_h)_0 + (\boldsymbol{a} \cdot \nabla u_h, v_h)_0 + \sigma(u_h, v_h)_0$$

$$- \sum_{T \in \mathcal{T}_h} \tau\left(\dfrac{\partial u_h}{\partial t} - \varepsilon\Delta u_h + \boldsymbol{a} \cdot \nabla u_h + \sigma u_h, -\varepsilon\Delta v_h - \dfrac{\boldsymbol{a} \cdot \nabla v_h}{\gamma} + \sigma v_h\right)_{0,T}$$

$$= (f, v_h)_0 - \sum_{T \in \mathcal{T}_h} \tau\left(f, -\varepsilon\Delta v_h - \dfrac{\boldsymbol{a} \cdot \nabla v_h}{\gamma} + \sigma v_h\right)_{0,T} \quad \forall\, v_h \in \mathcal{V}_1, \tag{28}$$

where the stabilization parameters τ and γ are given in (6) and (7) in Section 2. After that, we use the time-discretization scheme such as the classical backward Euler method or the Crank-Nicolson method to discrete the time variable of the semi-discrete formulation (28). Here, we remark again that in adaptive computations, we may replace the stabilization parameters τ and γ by the elementwise stabilization parameters τ_T and γ_T that are defined in (11) and (12) in Remark 1 in Section 2.

In the literature, various stabilized FEMs have been proposed and analyzed for solving the time-dependent reaction-convection-diffusion problem (27). We refer the reader to the recent works [27, 28] and many references cited therein. However, it has been observed in, e.g., [29, 30, 31, 32], that the small time step may cause the instability when conventional stabilized finite element formulations are applied to solve time-dependent reaction-convection-diffusion problems. In what follows, we will consider two examples to illustrate that the newly proposed stabilization method is really stable and accurate, even if the diffusivity ε is very small and the reaction coefficient σ is large enough.

Example 4. In this example, we investigate the *L*-shaped front problem which is quoted from [31]. Let $\Omega = (0, 1) \times (0, 1)$ be the spatial domain. We consider the initial-boundary value problem (27) with the zero source term $f = 0$, the small diffusivity $\varepsilon = 10^{-6}$, the zero reaction coefficient $\sigma = 0$, and the constant convection field $\boldsymbol{a} = (\frac{\sqrt{2}}{2}, \frac{\sqrt{2}}{2})^\top$. The initial and boundary conditions are described in Figure 10. We use the P_1 elements on a uniform triangular mesh as that described in Example 1 and $h^* = 1/40$, $h = \sqrt{2}h^*$, various time steps $\Delta t = h^*, h^*/4, h^*/8$, to produce the stabilized finite element approximations, where the simple backward Euler method is applied to the time-discretization for the semi-discrete formulation (28). The numerical results at $t = 0.25$ and $t = 1.5$ are respectively depicted in Figure 11, from which we can observe that our approach can produce reasonable results with a high stability for CFL numbers of 1, 0.25, and 0.125.
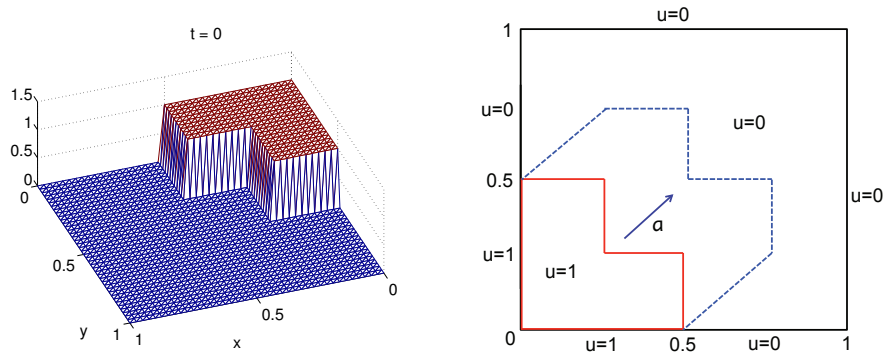
Figure 10. Initial and boundary conditions of Example 4 .
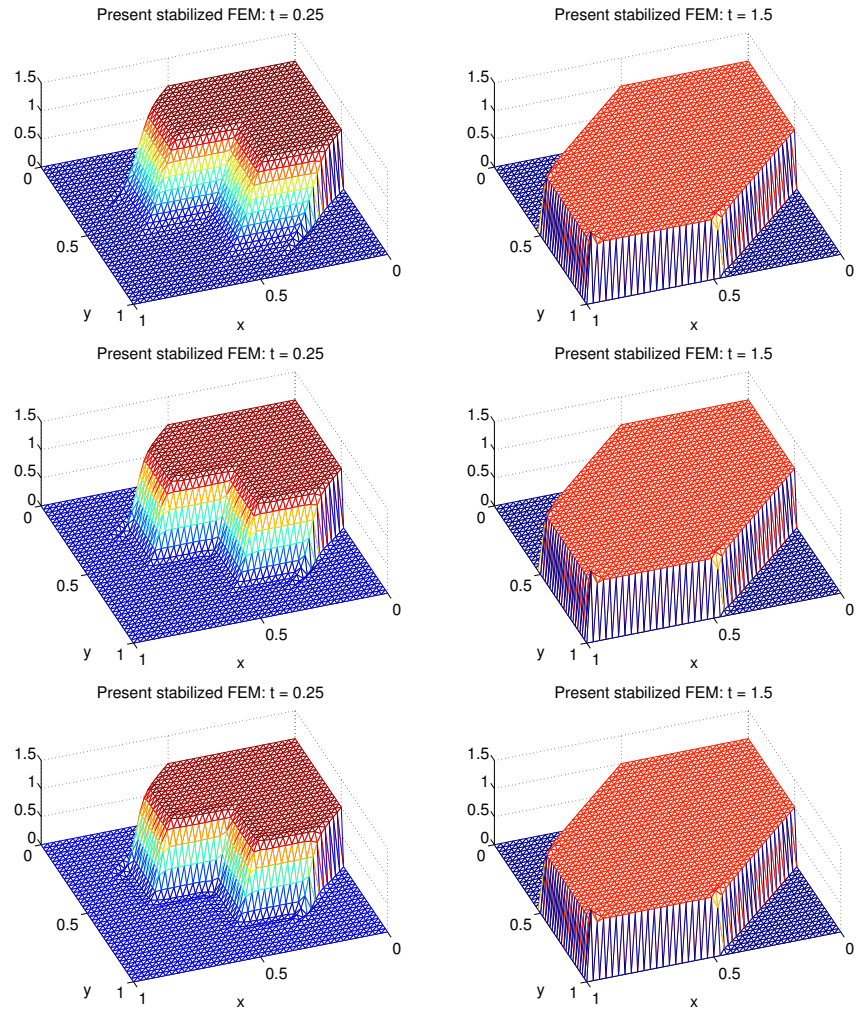
Figure 11. Elevation plots of the stabilized finite element solutions of Example 4 with $\varepsilon = 10^{-6}$ and $\sigma = 0$ at $t = 0.25$ and $t = 1.5$, using P_1 elements, $h^* = 1/40$, $h = \sqrt{2}h^*$ and time step $\Delta t = h^*$ (top row), $\Delta t = h^*/4$ (middle row) and $\Delta t = h^*/8$ (bottom row).

Example 5. This is a hump problem taken from [33]. Consider the time-dependent convection-diffusion-reaction problem (27) with the small diffusivity $\varepsilon = 10^{-6}$, the convection field $\boldsymbol{a} = (2, 3)^\top$ and the initial function $u_0 \equiv 0$ in the spatial domain $\Omega := (0, 1) \times (0, 1)$. We assume that the problem has an exact solution in the form

$$u(t, x, y) = 16 \sin(\pi t)x(1 - x)y(1 - y)\left(\frac{1}{2} + \frac{\arctan[2\varepsilon^{-1/2}(0.25^2 - (x - 0.5)^2 - (y - 0.5)^2)]}{\pi}\right).$$

This is a hump changing its height periodically in time and a strong interior layer may appear (cf. Figure 12 and Figure 14). Note that the exact solution u is independent of the reaction coefficient σ.

In the numerical simulations, we first use the uniform triangular mesh with $h^* = 1/128$ and take the mesh parameter $h = \sqrt{13/9}h^*$, which is the largest diameter of element T in the direction of $\boldsymbol{a} = (2, 3)^\top$. We take a small time step length $\Delta t = 10^{-3}$ and consider the cases of $\sigma = 1000$ and $\sigma = 1$. The numerical results at $t = 0.5$ are depicted in Figure 12. From the numerical results in Figure 12, we find that our approach can achieve a good approximation with a high stability for $\sigma = 1000$. However, only a reasonable result can be obtained for the small reaction coefficient $\sigma = 1$, since there is still a little oscillation near the interior layer region and this behavior is similar to the most typical methods studied in [33]. In order to test the performance of our approach in adaptive computations, we next consider the scheme on a given unstructured adaptive mesh which is depicted in Figure 13. The numerical results are shown in Figure 14. We find that for both $\sigma = 1000$ and $\sigma = 1$, our approach can achieve a rather good accuracy and the stability has been greatly improved for the case of small reaction coefficient $\sigma = 1$.
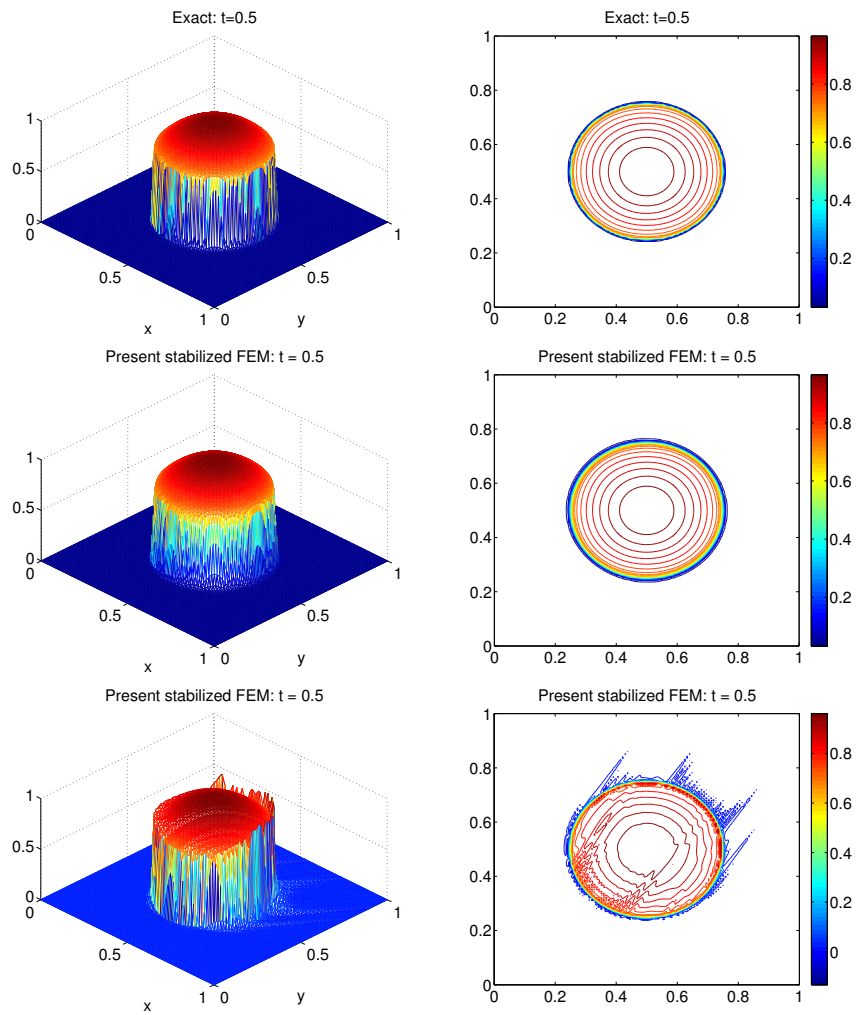
Figure 12. Elevation and contour plots of the exact and the stabilized finite element solutions of Example 5 with $\varepsilon = 10^{-6}$, $\sigma = 1000$ (middle row) and $\sigma = 1$ (bottom row) at $t = 0.5$, using P_1 elements, $h^* = 1/128$, $h = \sqrt{13/9} h^*$ and time step $\Delta t = 10^{-3}$.
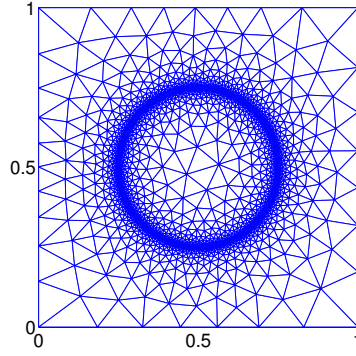
Figure 13. An unstructured adaptive mesh containing 4566 triangles and 2300 nodes for Example 5.
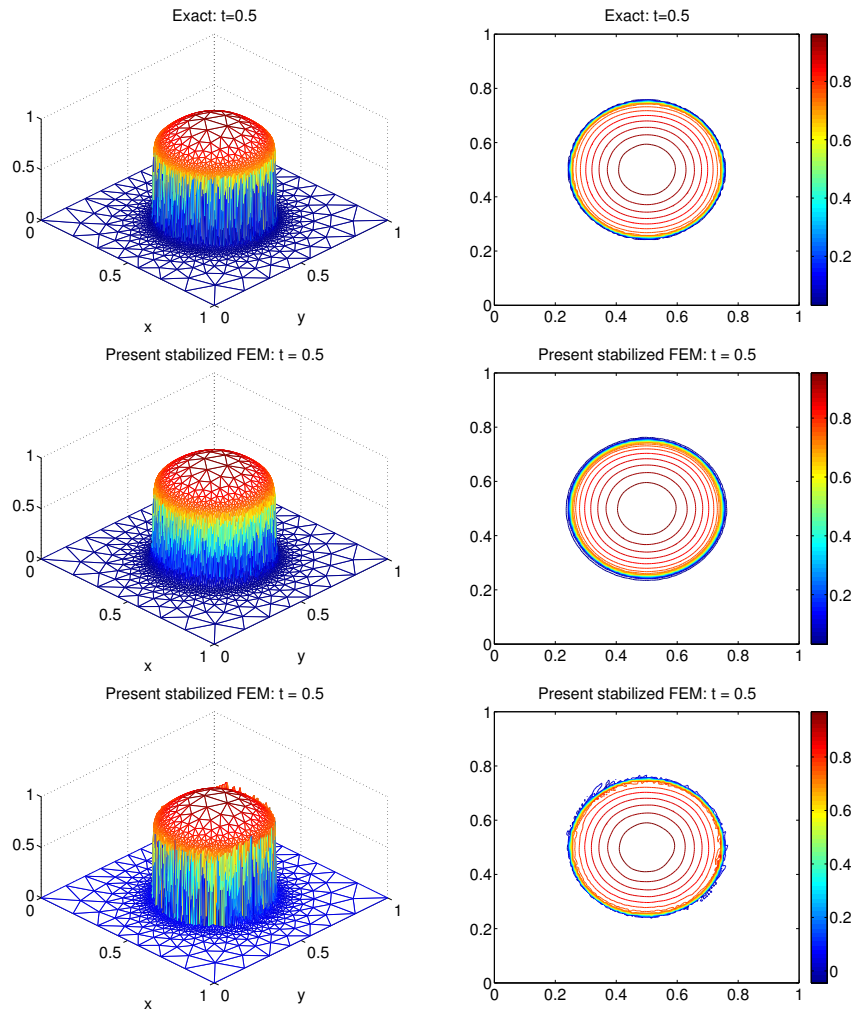
Figure 14. Elevation and contour plots of the exact and stabilized finite element solution of Example 5 with $\varepsilon = 10^{-6}$, $\sigma = 1000$ (middle row) and $\sigma = 1$ (bottom row) at $t = 0.5$, using P_1 elements on the unstructured adaptive mesh given in Figure 13 and time step $\Delta t = 10^{-3}$.

22

6. Summary and conclusions

In this paper, we have proposed and analyzed a new stabilized FEM using continuous piecewise P_1 (or Q_1) elements to approximate solution of reaction-convection-diffusion equations with arbitrary magnitudes of reaction and diffusion. The most important feature of the proposed method is that the test function in the stabilization term is taken in the adjoint-operator-like form $-\varepsilon \Delta v - (\boldsymbol{a} \cdot \nabla v)/\gamma + \sigma v$, where the stabilization parameter γ is appropriately designed to adjust the convection strength to achieve high accuracy and stability. We have derived the stability estimates for the finite element solutions and then established the explicit dependence of L^2 and H^1 error bounds on ε, $\|\boldsymbol{a}\|$, σ and h, from which we have found that the proposed method is suitable for a wide range of mesh Péclet (Pe_h) numbers and mesh Damköhler (Da_h) numbers. Indeed, if the diffusivity ε is sufficiently small with $\varepsilon < \|\boldsymbol{a}\|h$ (i.e., $Pe_h > 1/2$) and the reaction coefficient σ is large enough such that $\|\boldsymbol{a}\| < \sigma h$ (i.e., $Da_h > 1$), then the method exhibits optimal convergence rates in both L^2 and H^1 norms. On the other hand, for a small reaction coefficient satisfying $\|\boldsymbol{a}\| \geq \sigma h$ (i.e., $Da_h \leq 1$), the method behaves like the well-known SUPG method. We have performed several numerical tests of layer problems, and numerical results confirm the error estimates of the proposed method. We have also found that the proposed method can work very well for the computations on unstructured and adaptive meshes, provided the stabilization parameters are directly redefined element-by-element. Finally, we have applied the method to two typical problems of time-dependent reaction-convection-diffusion equations and the simulation results have shown the efficiency of the proposed approach. The analysis of this issue will be subject for future work.

Acknowledgments

References

[1] H. C. Elman, D. J. Silvester, and A. J. Wathen, *Finite Elements and Fast Iterative Solvers: with Applications in Incompressible Fluid Dynamics*, Oxford University Press, New York, 2005.

[2] C. Johnson, *Numerical Solution of Partial Differential Equations by the Finite Element Method*, Cambridge University Press, Cambridge, 1987.

[3] K. W. Morton, *Numerical Solution of Convection-Diffusion Problems*, Chapman & Hall, London, 1996.

[4] H.-G. Roos, M. Stynes, and L. Tobiska, *Numerical Methods for Singularly Perturbed Differential Equations*, Springer, New York, 1996.

[5] M. Stynes, Steady-state convection-diffusion problems, *Acta Numerica*, 2005, pp. 445-508.

[6] A. N. Brooks and T. J. R. Hughes, Streamline upwind/Petrov-Galerkin formulations for convective dominated flows with a particular emphasis on the incompressible Navier-Stokes equations, *Comput. Methods Appl. Mech. Engrg.*, 32 (1982), pp. 199-259.

[7] L. P. Franca, S. L. Frey, and T. J. R. Hughes, Stabilized finite element methods: I. application to the advective-diffusive model, *Comput. Methods Appl. Mech. Engrg.*, 95 (1992), pp. 253-276.

[8] L. P. Franca and S. L. Frey, Stabilized finite element methods: II. the incompressible Navier-Stokes equations, *Comput. Methods Appl. Mech. Engrg.*, 99 (1992), pp. 209-233.

[9] P.-W. Hsieh and S.-Y. Yang, On efficient least-squares finite element methods for convection-dominated problems, *Comput. Methods Appl. Mech. Engrg.*, 199 (2009), pp. 183-196.

[10] T. J. R. Hughes, Multiscale phenomena: Green's functions, the Dirichlet-to-Neumann formulation, subgrid scale models, bubbles and the origins of stabilized methods, *Comput. Methods Appl. Mech. Engrg.*, 127 (1995), pp. 387-401.

[11] T. J. R. Hughes, L. P. Franca, and G. M. Hulbert, A new finite element formulation for computational fluid dynamics: VIII. the Galerkin/least-squares method for advective-diffusive equations, *Comput. Methods Appl. Mech. Engrg.*, 73 (1989), pp. 173-189.

[12] L. P. Franca, G. Hauke, and A. Masud, Revisiting stabilized finite element methods for the advective-diffusive equation, *Comput. Methods Appl. Mech. Engrg.*, 195 (2006), pp. 1560-1572.

[13] T. E. Tezduyar and Y. J. Park, Discontinuity capturing finite element formulations for nonlinear convection-diffusion-reaction equations, *Comput. Methods Appl. Mech. Engrg.*, 59 (1986), pp. 307-325.

[14] F. Brezzi and A. Russo, Choosing bubbles for advection-diffusion problems, *Math. Models Meth. Appl. Sci.*, 4 (1994), pp. 571-587.

[15] F. Brezzi, L. P. Franca, and A. Russo, Further considerations on residual-free bubbles for advective-diffusive equations, *Comput. Methods Appl. Mech. Engrg.*, 166 (1998), pp. 25-33.

[16] L. P. Franca, J. V. A. Ramalho, and F. Valentin, Multiscale and residual-free bubble functions for reaction-advection-diffusion problems, *Int. J. Multiscale Comput. Eng.*, 3 (2005), pp. 297-312.

[17] P.-W. Hsieh and S.-Y. Yang, A novel least-squares finite element method enriched with residual-free bubbles for solving convection-dominated problems, *SIAM J. Sci. Comput.*, 32 (2010), pp. 2047-2073.

[18] L. P. Franca and C. Farhat, Bubble functions prompt unusual stabilized finite element methods, *Comput. Methods Appl. Mech. Engrg.*, 123 (1995), pp. 299-308.

[19] L. P. Franca and F. Valentin, On an improved unusual stabilized finite element method for the advective-reactive-diffusive equation, *Comput. Methods Appl. Mech. Engrg.*, 190 (2000), pp. 1785-1800.

[20] H.-Y. Duan, A new stabilized finite element method for solving the advection-diffusion equations, *J. Comput. Math.*, 20 (2002), pp. 57-64.

[21] G. Hauke, G. Sangalli, and M. H. Doweidar, Combining adjoint stabilized methods for the advection-diffusion-reaction problem, *Math. Models Methods Appl. Sci.*, 17 (2007), pp. 305-326.

[22] H.-Y. Duan, P.-W. Hsieh, Roger C.E. Tan, and S.-Y. Yang, Analysis of a new stabilized finite element method for the reaction-diffusion-convection equations with a large reaction coefficient, *Comput. Methods Appl. Mech. Engrg.*, 247-248 (2012), pp. 15-36.

[23] S. C. Brenner and L. R. Scott, *The Mathematical Theory of Finite Element Methods*, Springer-Verlag, New York, 1994.

[24] P. G. Ciarlet, *The Finite Element Method for Elliptic Problems*, North-Holland Publishing Company, Amsterdam, 1987.

[25] V. Girault and P. A. Raviart, *Finite Element Methods for Navier-Stokes Equations: Theory and Algorithms*, Springer-Verlag, New York, 1986.

[26] F. Hecht, O. Pironneau, J. Morice, A. Le Hyaric, and K. Ohtsuka, *FreeFem++, Third Edition, Version 3.19*, 2012, http://www.freefem.org/ff++/.

[27] P. Nadukandi, E. Oñate, and J. Garcia, A high-resolution Petrov-Galerkin method for the 1D convection-diffusion-reaction problem, *Comput. Methods Appl. Mech. Engrg.*, 199 (2010), pp. 525-546.

[28] P. Nadukandi, E. Oñate, and J. Garcia, A high-resolution Petrov-Galerkin method for the convection-diffusion-reaction problem: Part II-A multidimensional extension, *Comput. Methods Appl. Mech. Engrg.*, 213-216 (2012), pp. 327-352.

[29] I. Harari, Stability of semidiscrete formulations for parabolic problems at small time steps, *Comput. Methods Appl. Mech. Engrg.*, 193 (2004), pp. 1491-1516.

[30] P. B. Bochev, M. D. Gunzburger, and R. B. Lehoucq, On stabilized finite element methods for the Stokes problem in the small time step limit, *Int. J. Numer. Meth. Fluids*, 53 (2007), pp. 573-597.

[31] M.-C. Hsu, Y. Bazilevs, V. M. Calo, T. E. Tezduyar, and T. J. R. Hughes, Improving stability of stabilized and multiscale formulations in flow simulations at small time steps, *Comput. Methods Appl. Mech. Engrg.*, 199 (2010), pp. 828-840.

[32] H.-Y. Duan, P.-W. Hsieh, Roger C. E. Tan, and S.-Y. Yang, Analysis of the small viscosity and large reaction coefficient in the computation of the generalized Stokes problem by a novel stabilized finite element method, *Comput. Methods Appl. Mech. Engrg.*, 271 (2014), pp. 23-47.

[33] V. John and E. Schmeyer, Finite element methods for time-dependent convection-diffusion-reaction equations with small diffusion, *Comput. Methods Appl. Mech. Engrg.*, 198 (2008), pp. 475-494.